

Journal Pre-proof



WNT Oncogenic Transcription Requires MYC Suppression of Lysosomal Activity and EPCAM Stabilization in Gastric Tumours

Patrizia Mulè, Daniel Fernandez-Perez, Simona Amato, Daria Manganaro, Paola Oldani, Stefania Brandini, Giuseppe Diaferia, Alessandro Cuomo, Camilla Recordati, Chiara Soriani, Ambra Dondi, Marika Zanotti, Samantha Rustichelli, Andrea Bisso, Salvatore Pece, Simona Rodighiero, Gioacchino Natoli, Bruno Amati, Karin Johanna Ferrari, Fulvio Chiacchiera, Diego Pasini

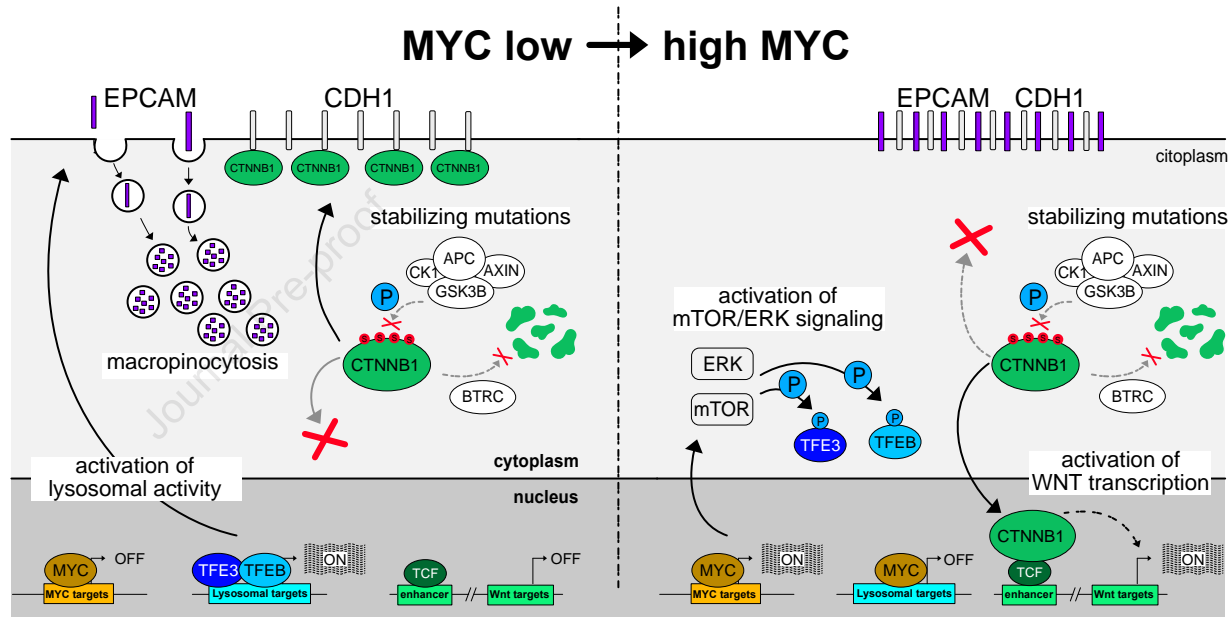
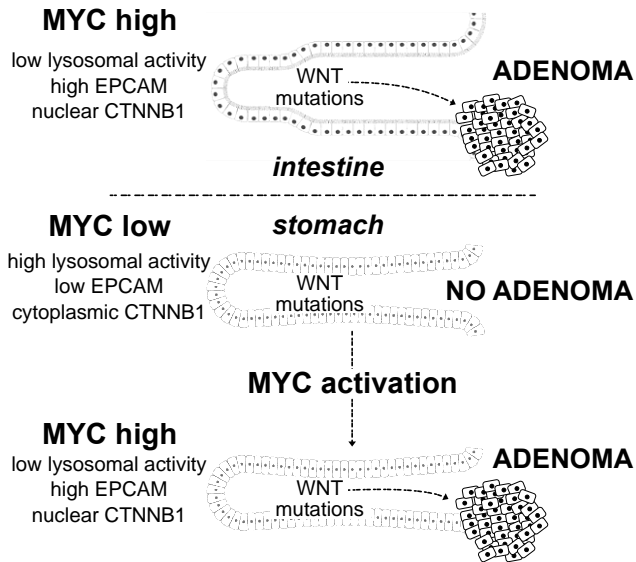
PII: S0016-5085(24)05182-5
DOI: <https://doi.org/10.1053/j.gastro.2024.06.029>
Reference: YGAST 66319

To appear in: *Gastroenterology*
Accepted Date: 18 June 2024

Please cite this article as: Mulè P, Fernandez-Perez D, Amato S, Manganaro D, Oldani P, Brandini S, Diaferia G, Cuomo A, Recordati C, Soriani C, Dondi A, Zanotti M, Rustichelli S, Bisso A, Pece S, Rodighiero S, Natoli G, Amati B, Ferrari KJ, Chiacchiera F, Pasini D, WNT Oncogenic Transcription Requires MYC Suppression of Lysosomal Activity and EPCAM Stabilization in Gastric Tumours, *Gastroenterology* (2024), doi: <https://doi.org/10.1053/j.gastro.2024.06.029>.

This is a PDF file of an article that has undergone enhancements after acceptance, such as the addition of a cover page and metadata, and formatting for readability, but it is not yet the definitive version of record. This version will undergo additional copyediting, typesetting and review before it is published in its final form, but we are providing this version to give early visibility of the article. Please note that, during the production process, errors may be discovered which could affect the content, and all legal disclaimers that apply to the journal pertain.

© 2024 by the AGA Institute



WNT Oncogenic Transcription Requires MYC Suppression of Lysosomal Activity and EPCAM Stabilization in Gastric Tumours

Patrizia Mulè^{1,4}, Daniel Fernandez-Perez^{1,4}, Simona Amato¹, Daria Manganaro¹, Paola Oldani¹, Stefania Brandini¹, Giuseppe Diaferia¹, Alessandro Cuomo¹, Camilla Recordati², Chiara Soriani¹, Ambra Dondi¹, Marika Zanotti¹, Samantha Rustichelli¹, Andrea Bisso¹, Salvatore Pece¹, Simona Rodighiero¹, Giocchino Natoli¹, Bruno Amati¹, Karin Johanna Ferrari¹, Fulvio Chiacchiera³ and Diego Pasini^{1,2,5,6}.

Affiliations:

- 1) IEO, European Institute of Oncology IRCCS, Department of Experimental Oncology, Via Adamello 16, 20139 Milan, Italy.
- 2) University of Milan, Department of Health Sciences, Via A. di Rudini 8, 20142 Milan, Italy
- 3) University of Trento, Department of Cellular, Computational and Integrative Biology (CIBIO), 38123 Trento, Italy
- 4) These authors contributed equally to this work
- 5) Lead contact
- 6) Correspondence to: diego.pasini@ieo.it

Corresponding authors contact information:

Prof. Diego Pasini

Via Adamello, 16. 20139, Milano. Italy.

Phone: +39 02 94375139

e-mail: diego.pasini@ieo.it

Conflict of interest statement: All authors declare no competing interests.

Authors contributions: PM performed the experiments. DFP performed the bioinformatic analyses. SB and GD performed the LCM. AC performed the MS analysis. DM provided support with organoids. SA and PO provided support with histology. CS, AD and SR provided support for human data acquisition and analysis. CR performed the pathological evaluation. MZ and SR supported with mice handling and genotyping. KJF organized the mouse colony and genetic strategies. GN provided LCM knowhow. SP provided the human patient histological samples. AB and BA provided experimental, knowhow and intellectual support. FC performed in vivo cooperation experiments and supported project strategy. DP and PM designed the experiments and prepared the manuscript.

Acknowledgments:

We thank Carmine Settembre and Sara Sigismund for discussion and experimental suggestions; Andrea Francesco Benvenuto and Daniela Amorelli for providing reagents and experimental support; all members of the Pasini's laboratory for discussion. DP work was supported by grants from the European Research Council, ERC (EC-H2020-ERC-CoG-DissectPcG: 725268); the Italian Association for Cancer Research, AIRC (IG-2017-20290 and IG-2022-27694) and the Worldwide Cancer Research (WWCR; 22-0027). ST work was supported by grants from AIRC (MFAG 2021-26131) and Fondazione Cariplo (Cariplo Giovani 2020-3576). FC work was supported by grants from AIRC (MFAG-20344) and WWCR (23-0321). DFP, DM and SA were supported by individual fellowships from AIRC. SR was supported by a fellowship from the Italian Ministry of University and Research (PNRR Borse DM 351). PM, SA, DFP, and SR were PhD students within the European School of Molecular Medicine (SEMM).

Data and code availability: All raw NGS data generated in this study have been deposited at the NCBI Gene Expression Omnibus (GEO) repository accession: GSE231581. Any additional information required to reanalyze the data reported in this work is available from the lead contact upon request.

Abstract***Background and aims***

WNT signaling is central to spatial tissue arrangement, regulating stem cell activity, and represents the hallmark of gastrointestinal cancers. While its role in driving intestinal tumors is well characterized, WNT's role in gastric tumorigenesis remains elusive.

Methods

We have developed mouse models to control the specific expression of an oncogenic form of B-CATENIN in combination with MYC activation in *Lgr5*⁺ cells of the gastric antrum. We used multi-omics approaches applied *in vivo* and in organoid models to characterize their cooperation in driving gastric tumorigenesis.

Results

We report that constitutive B-CATENIN stabilization in the stomach has negligible oncogenic effects and requires MYC activation to induce gastric tumour formation. While physiologically low MYC levels in gastric glands limit B-CATENIN transcriptional activity, increased MYC expression unleashes the WNT oncogenic transcriptional program, promoting B-CATENIN enhancer invasion without a direct transcriptional cooperation. MYC activation induces a metabolic rewiring that suppresses lysosomal biogenesis through mTOR and ERK activation and MiT/TFE inhibition. This prevents EPCAM degradation by macropinocytosis, promoting B-CATENIN chromatin accumulation and activation of WNT oncogenic transcription.

Conclusion

Our results uncovered a new signaling framework with important implications for the control of gastric epithelial architecture and WNT-dependent oncogenic transformation.

Keywords:

WNT signalling, B-CATENIN, CTNNB1, MYC, gastric cancer, LGR5 positive cells, transcription, chromatin

Introduction

WNT signaling plays an essential role in regulating gastrointestinal (GI) homeostasis¹. The stomach and intestine share the expression of the WNT target gene *Lgr5*, a receptor for R-spondin ligands secreted in stem cell niches^{2,3}. Along the intestinal tracts, *Lgr5* marks a population of cells responsible for tissue renewal³. In the stomach corpus, *Lgr5* is expressed by a population of chief cells acting as an injury-responsive stem cell reservoir⁴. Similarly, in the gastric pyloric-antrum, *Lgr5* expression marks slowly cycling basal mucous cells with stem cell properties that contribute to homeostatic gland renewal^{2,5,6}. The pyloric stomach additionally harbors a population of rapidly cycling isthmus stem cells characterized by high expression of the WNT target genes *Axin2* and *Lgr4* but low expression of *Lgr5*^{7,8}. WNT ligands coordinate cell proliferation and differentiation by regulating the intracellular levels of B-CATENIN (CTNNB1)⁹. Activation of canonical WNT receptors LRP4/5 and FRZ triggers the release of CTNNB1 from the destruction complex, preventing its GSK3B-mediated phosphorylation and TRCP-mediated degradation. Increased CTNNB1 levels allow its nuclear accumulation, where it associates with the TCF/LEF family of transcription factors, activating WNT transcription programs⁹. Approximately 90% of colorectal cancers (CRCs) and 50% of gastric tumors (GCs) display WNT-activating mutations^{10,11} that prevent CTNNB1 degradation. This results in its nuclear accumulation, which triggers a constitutive overactivation of a WNT transcriptional program¹². Truncating mutations of APC or missense mutations abrogating GSK3B phosphorylation of CTNNB1 induce the development of adenomas in the mouse intestine, perturbing stem cell proliferation, migration, and differentiation^{13,14}. WNT mutations are also frequent in gastric cancers, but their role remains less characterized. Differently from the intestine, APC loss in basal LGR5+ cells was inefficient, and mice developed some adenomas only after long latencies^{2,6}, suggesting that additional genetic or epigenetic events could be required.

The MYC proto-oncogene is considered a WNT-target in CRC cell lines¹⁵ and its activity is essential but not sufficient for WNT-dependent adenoma formation in the mouse intestine¹⁶. The oncogenic role of MYC is pleiotropic, and its genetic or epigenetic activation represents a hallmark across the majority of tumors¹⁷. MYC is a basic helix-loop-helix zipper (bHLHZ) TF that regulates the expression of thousands of genes, coordinating a wide range of context-dependent cellular responses that promote cell growth, proliferation, and metabolic rewiring¹⁸. In gastric cancers, MYC nuclear overexpression was reported in >75% of cases with frequent MYC locus amplifications, promoter hypomethylation, and FBXW7 inactivating mutations^{19,20}.

Our study shows that low MYC levels limit adenoma development in the stomach antrum, and its activation cooperates with CTNNB1 mutations in the formation of gastric tumors. This involves MYC suppression of lysosomal biogenesis that prevents EPCAM degradation by macropinocytosis, which promotes CTNNB1 chromatin invasion to activate WNT oncogenic transcription.

Materials and methods

Animal procedures

Mouse work was in accordance with the standards of the Italian law (D.L.vo 116/92 and following additions) and the European directive 86/609 regarding the protection of animals used for experimental and scientific purposes. Genotyping and Cre activation details are available as supplemental information.

Intestinal crypts and gastric glands isolation

Crypts and pyloric glands were isolated by EDTA-mediated $\text{Ca}^{2+}/\text{Mg}^{2+}$ chelation followed by mechanical disaggregation as previously reported ²¹. Details are available as supplementary information.

Organoids culture and manipulation

Mouse organoids were generated as previously described ²¹ and grown in the presence of R-spondin1 and Wnt3a (where indicated). GI single cells were transduced with concentrated lentiviral particles and seeded on top of polymerized Matrigel as previously described ²². Culture conditions and details are available as supplementary information.

Laser Capture Microdissection and Mass spectrometry analysis

Laser Capture Microdissection (LCM) was performed on FFPE sections on polyethylene naphthalate membrane (PEN) slides (Leica cat. 11600289) photoactivated in an UV crosslinker for 30 min (BLX-254, Bio-Link). For mass spectrometry, LCM samples were digested with PreOmics iST preparation kit, following instructions. All analytical details are available in supplementary information.

Single cell RNA sequencing

Single cell RNA-seq analysis was performed on gastric pyloric cells following the 10x Genomics Single Cell Gene Expression Flex instructions and sequenced on Illumina Novaseq 6000. Reads were processed using the 10X Genomics workflow (v4.0). More details in supplementary information.

Bulk RNA sequencing

RNA-seq libraries were prepared using a custom Smart-seq2 procedure previously described ²³. All details are available as supplementary information.

Chromatin Immunoprecipitation-Sequencing (ChIP-seq)

ChIP assays were performed as previously described ²⁴. DNA was purified with PCR purification Kit (Qiagen) and used for library preparation and sequenced using NovaSeq 6000. See supplementary information for details.

Results

MYC cooperates with CTNNB1 to drive gastric tumorigenesis

We employed an *Lgr5* eGFP-IRES-CreERT2 knock-in model (referred to as *Lgr5* KI; Figure S1A) for CRE recombinase activation in gastrointestinal *Lgr5*-expressing cells³. This allows us to visualize and purify both gastric (GC) and intestinal (IC) *Lgr5*⁺ cells, taking advantage of GFP expression. This was combined with a *Ctnnb1*^{ex3}/WT conditional allele (hereafter referred to as *Ctnnb1*, Figure S1A) to induce *Ctnnb1* exon 3 deletion, which leads to CTNNB1 stabilization and adenoma formation across the intestine¹³.

We induced WNT activation in *Lgr5*⁺ cells by IP TAM injections in 8-12-week-old sex-matched mice. Histological analysis 30 days after TAM administration (PTI) showed the development of multiple adenomas (Figure 1A) enriched by GFP⁺ cells (Figure 1B and 1C) in the small intestine as reported¹³. However, the gastric pyloric epithelium maintained a normal morphology with no signs of transformation (Figure 1A). The GFP⁺ cells were normally localized at the bottom of gastric glands, and their number was unchanged compared to wild-type (WT) mice (Figure 1B and 1C). This agrees with the long tumor latency observed by APC loss in the same *Lgr5*⁺ GC⁶, suggesting that WNT mutations are not sufficient to transform the gastric epithelium.

MYC activity is required for WNT-driven intestinal adenoma formation¹⁶. This prompts us to evaluate MYC expression in the gastric mucosa. RNA-seq analyses and RT-qPCR validation in WT mice demonstrated that *Myc* expression was at least 5 times lower in *Lgr5*⁺ GC compared to IC (Figure 1D and Table S1). Immunofluorescence (IF) staining confirmed clear MYC expression in *Lgr5*⁺ IC that was barely detectable in the stomach (Figure 1E). CTNNB1 stabilization (*Ctnnb1* mice 30 days PTI) showed that both *Myc* transcription (Figure S1B) and its protein levels (Figure S1C and S1D) remained unaltered. This shows that MYC is not a target of WNT signaling as previously proposed¹⁵ and that its low expression could be limiting for WNT-driven tumorigenesis in the stomach.

We used a *Rosa26*-CAG lox-STOP-lox-*Myc*-ires-*hCD2* allele²⁵ for MYC overexpression (Figure S1A; referred to as *CAG-Myc*) crossed with the *Lgr5* KI in the presence or absence of the *Ctnnb1* allele. Histological analysis of the gastric epithelium 30 days PTI demonstrated that increased MYC activation synergizes with CTNNB1, leading to aggressive development of multiple high-grade adenomas (Figure 1F, 1G, and S2A-E). Neoplastic formations were not observed when MYC or CTNNB1 were activated alone. While CTNNB1 had negligible effects on gastric histology, MYC overexpression induced gland hyperplasia (Figure 1F, 1G, and S2A-C).

Transgene activation specifically occurred in *Lgr5*⁺ basal mucous cells at the gland bottom. LacZ tracing (*R26*^{ISILacZ})²⁶ at day 2 from TAM administration demonstrated that 80% of LacZ⁺ cells were located at the gland base and progressed across the isthmus over time, labeling the entire gastric glands

(Figure 1H and S3A). This was associated with initial MYC activation in basal *Lgr5*⁺ GC that progressed to the top of the gastric glands and correlated with KI67 positivity (Figure S3B and S3C).

MYC and CTNNB1 expand *Lgr5*⁺ GC activating a WNT transcriptional program, suppressing differentiation

KI67 and GFP co-expression showed extensive proliferation of *Lgr5*⁺ (GFP⁺) cells across all neoplastic areas of *CAG-Myc/Ctnnb1* mice (Figure 2A). FACS quantifications confirmed that GFP⁺ cells (thus *Lgr5*⁺) were >10 times more abundant in *CAG-Myc/Ctnnb1* mice compared to all other models (Figure 2B and S4A). This occurred without the expression of *Lgr5*⁺ basal-cell secretory markers and had a negative effect on the Pit lineage (Figure 2C and S4B). Importantly, MYC activation alone stimulated an expansion of the proliferative isthmus, whereas the *Lgr5*⁺ cells remained at the gland bottom as in WT and *Ctnnb1* mice (Figure 2A).

RNA-seq analysis in *Lgr5*⁺ cells 21 days PTI confirmed this, showing that MYC and CTNNB1 co-activation induced extensive transcriptional changes (Figure 2D, S4C, and Table S1) linked to WNT signaling and gastric cancer-specific gene sets (Figure 2E and S4D). To extend this, we employed single-cell RNA sequencing (scRNA-seq) of the gastric pyloric regions at 30 days PTI (Figure S4E). After annotating all cells based on known markers (Figure 2F, S4F, and Table S2), we identified two specific clusters: one present in *CAG-Myc* and *CAG-Myc/Ctnnb1* mice (referred to as the Myc cluster) and another specific for *CAG-Myc/Ctnnb1* (referred to as the MycBCat cluster) (Figure 2F). High human CD2 positivity for both clusters confirmed their transgenic origin (Figure S4G). These clusters were not present in *Ctnnb1* mice, which displayed no differences from the WT control.

The Myc cluster was marked by *Gstm3* expression and known MYC targets (*Ncl*, *Smpdl3b*). It was highly proliferative (*Pcna*⁺ and *Mki67*⁺) and did not express markers associated with gastric cell types, including *Lgr5*⁺ basal cells (Figure S4H). The MycBCat cluster was also highly proliferative but positive for *Lgr5* (Figure 2G). Indeed, the MycBCat cluster contained the highest number of *Lgr5*⁺ proliferating cells (Figure S4I). These cells were different from normal *Lgr5*⁺ basal cells, which are quiescent and express secretory genes such as *Muc6* and *Gif* (Figure S4J). The MycBCat cluster also expressed high levels of CRC-related genes (*Ifitm1*, *Ifitm3*, *Bex1*, *Igfbp4*), markers of oncogenic WNT activation (i.e., *Notum*, *Axin2*, *Sp5*, *Rnf43*), and was enriched for a WNT-related intestinal tumor signature (Figure 2G and S4K). This was confirmed by bulk RNA-seq analysis, where the MycBCat gene signature was specifically activated in *CAG-Myc/Ctnnb1* *Lgr5*⁺ GC together with a suppression of differentiation (Figure 2H).

Using laser-capture microdissection (LCM; Figure S5A) coupled with mass spectrometry (Figure S5B), we further confirmed that the proteomic signature of *CAG-Myc/Ctnnb1* tumors was specifically enriched in the MycBCat cluster (Figure 2I). Immunohistochemistry (IHC) for IFITM3 further validated these results (Figure 2J), demonstrating that the MycBCat cluster represents gastric neoplastic

cells. Indeed, this cluster signature was highly expressed in a subset of gastric cancers (Figure S5C) and correlated with lower patient survival (Figure S5D).

These results suggest that MYC and CTNNB1 cooperate to rewire *Lgr5*⁺ quiescent cells and generate undifferentiated gastric tumors characterized by high WNT activity with an intestinal stem-like identity.

MYC and CTNNB1 cooperation is preserved in gastric organoids models

Gastric organoids change their morphology in relation to the levels of WNT activity. In the presence of Wnt3a stimulation, gastric organoids acquire a "gland-type" morphology filled with small buds and a low number of *Muc5ac*⁺ Pit-like cells. Upon WNT withdrawal, organoids switch to a "pit-type" cystic phenotype primarily made of Pit-like cells^{2,27}.

We derived organoids from *Ctnnb1*, *CAG-Myc*, and *CAG-Myc/Ctnnb1* gastric glands and grew them without Wnt3a to select CreERT2 expression. *Ctnnb1* and *CAG-Myc* organoids developed with a cystic morphology suggesting low WNT activity confirmed by RNA-seq (Figure 2K and 2L). However, while *Ctnnb1* organoids preserved the expression of basal mucous markers, these were suppressed in *CAG-Myc* organoids, demonstrating an expansion of cells reminiscent of *in vivo* gland dysplasia (Figure 2L and Table S3).

CAG-Myc/Ctnnb1 organoids were markedly different and grew with pronounced budding structures without Wnt3a, suggesting an intrinsic high WNT transcriptional activity (Figure 2K). RNA-seq confirmed this showing reduced Pit markers together with increased expression of proliferative markers and WNT targets. This further correlated with an increased expression of the MycBcat gene signature, demonstrating that gastric organoids reproduce MYC-CTNNB1 cooperation observed *in vivo* (Figure 2L).

MYC enhances WNT transcription by increasing CTNNB1 chromatin invasion

ChIP-seq analysis in organoids showed that, while MYC occupancy was unchanged in *Ctnnb1* and WT conditions, its chromatin association was enhanced when overexpressed (Figure 3A). The number of MYC-associated loci (peaks; $FDR \leq 10^{-5}$) was more than four times higher in *CAG-Myc* and *CAG-Myc/Ctnnb1* organoids (Figure S6A and Table S4). These peaks overlapped (Figure 3B), demonstrating that CTNNB1 activation did not alter MYC genomic occupancy.

In *Ctnnb1* organoids, the number of CTNNB1 ChIP-seq peaks only increased by ~2-fold (Figure 3C and S6B), suggesting that its stabilization was not sufficient to enhance chromatin occupancy. MYC co-activation increased this number by ~10 times, an effect that was not observed in the absence of CTNNB1 oncogenic stabilization (Figure 3C, 3D, S6B, and Table S4). Consistent with the expansion of progenitors with no WNT activity, *CAG-Myc* organoids lacked CTNNB1 chromatin association (Figure 3C and S6B).

In the stomach of *Ctnnb1* mice, CTNNB1 was mainly localized at the plasma membrane and efficiently translocated to the nucleus only when MYC was co-activated (*CAG-Myc/Ctnnb1*) (Figure 3E). This was different from the small intestine where CTNNB1 efficiently localized to the nucleus and accumulated to chromatin similarly to *CAG-Myc/Ctnnb1* gastric organoids (Figure S6C-E). This suggests that high MYC expression is required for CTNNB1 to invade its target loci to maintain WNT transcription in an active state.

CTNNB1 was primarily bound to enhancer elements distant from transcription start sites (TSS), while MYC showed a preference for TSS, leading to limited reciprocal overlap (Figure 3F-H). This restricts the ability to identify CTNNB1 direct target genes and to score for transcriptional cooperation. To overcome this limitation, we predicted direct targets by associating each MYC or CTNNB1 peak with the closest gene, regardless of its distance from TSS (Figure 3I). This generated a list of potential CTNNB1 targets, half of which were directly associated with MYC (Figure 3J and S6F). Consistent with their high WNT activity, the general expression of all CTNNB1 targets was activated exclusively in *CAG-Myc/Ctnnb1 Lgr5+* GC and gastric organoids (Figure 3J). However, this scored no correlation between transcriptional activation and MYC co-association (Figure 3J), suggesting that MYC regulates CTNNB1 chromatin accumulation with an indirect mechanism (Figure 3K).

MYC controls lysosomal biogenesis and autophagy across the gastrointestinal epithelium

The comparison of RNA-seq analyses of *Lgr5+* GC vs. IC showed a specific enrichment in the stomach for lysosomal and autophagy catabolic processes (Figure 4A, S7A, and S7B). MYC activity has already been linked to these processes in other systems²⁸⁻³² suggesting a role in their regulation across the gastrointestinal tract. Lysosome quantification by fluorescent staining (LysoTracker) confirmed that *Lgr5+* GC contained more lysosomes relative to the small intestine and colon (Figure 4B, S7C, and S7D). The increased LC3-II/LC3-I ratio and flux of gastric glands vs. intestinal crypts also indicated higher autophagy in the stomach (Figure 4C, S7E, and S7F). This was confirmed by the large number of P62 puncta detected by IF in gastric glands vs. intestinal crypts (Figure S7G), as well as by *Sqstm1* transcriptional silencing (P62 encoding gene), which led to lower P62 bulk levels³³ (Figure S7H).

Lysosomal biogenesis and autophagy were unaffected in *Lgr5+* GC of *Ctnnb1* mice but were suppressed in both *CAG-Myc* and *CAG-Myc/Ctnnb1* mice (Figure 4D and S8A-D). This suppression was specific to the stomach, as MYC activation had no effect in the small intestine and colon (Figure S8E). RNA-seq analysis in gastric organoids confirmed that the expression of lysosomal and autophagy-related genes was also specifically reduced in *CAG-Myc* and *CAG-Myc/Ctnnb1* (Figure 4E and S8F), consistent with reduced *Sqstm1* transcription (Figure S8G). Indeed, the specific activation of MYC in gastric organoids suppressed both lysosome biogenesis and autophagic activity (Figure 4F, 4G, and S8H-J). Together, this indicates that MYC levels negatively regulate the general lysosomal activity of the gastric mucosa.

Lysosomal biogenesis and autophagy are controlled by a common transcriptional program coordinated by the activity of the Microphthalmia family of bHLH-LZ (MiT/TFE) TFs³⁴. *Tfe3*, *Tfeb*, and *Mitf* were all expressed in gastric glands and organoids (Figure S9A), and their expression was not affected by MYC or CTNNB1 activation (Figure S9B). MiT/TFE and MYC recognize a common hexanucleoside E-BOX sequence (CACGTG)³⁴, suggesting potential genomic competition for the same loci. It was proposed that MYC could suppress lysosomal biogenesis by acting as a transcriptional repressor through direct competition with MiT/TFE association²⁸. Consistent with this, all MiT/TFE binding motifs were enriched underneath MYC peaks (Figure S9C). However, only ~30% of the DEGs linked to lysosome biogenesis and autophagy were direct MYC targets (Figure 4H and S9D).

MiT/TFE transcriptional activity can also be inhibited by phosphorylations that prevent their nuclear localization³⁴. This can involve mTOR, ERK, AKT, or GSK3B kinases that are controlled by signaling pathways previously linked to MYC activity³⁵. Indeed, mTORC1 was one of the most enriched GO terms in CAG-Myc organoids RNA-seq analyses (Figure S9E). Consistent with this, TFE3 and TFEB IFs showed nuclear exclusion when MYC was specifically overexpressed in gastric glands at 30 days PTI (Figure 4I, 4J and S9F). This suggests that MYC-dependent transcriptional rewiring could suppress lysosomal activity by preventing MiT/TFE nuclear access. Indeed, the inhibition of mTOR or ERK specifically increased lysosome biogenesis (Lysotracker) in CAG-Myc/Ctnnb1 gastric organoids (Figure S9G). These pathways act in parallel, as combined ERK and mTOR inhibition further increased lysosome content (Figure 4K). Moreover, MYC activation, but not CTNNB1 stabilization, activated both signaling pathways as measured by increased S6 and ERK phosphorylation (Figure 4L). Consistently, MYC inhibition in Ctnnb1 intestinal organoids (where MYC is already physiologically active) reduced S6 and ERK phosphorylation together with increased lysosome biogenesis (Lysotracker) (Figure 4M and 4N). This points to a direct connection between MYC activation of mTOR and ERK signaling and the suppression of lysosome biogenesis and autophagy.

MYC stabilizes EPCAM levels suppressing Macropinocytosis-dependent degradation

The LCM-MS proteomic analyses showed that the transmembrane protein EPCAM was upregulated in CAG-Myc and CAG-Myc/Ctnnb1 conditions (Figure 5A) in the absence of transcriptional changes (Table S1 and S3). EPCAM can destabilize CTNNB1:E-CADHERIN (CDH1) interaction at the plasma membrane, and its overexpression favors CTNNB1 nuclear accumulation^{36,37}. We found that EPCAM levels were high in the small intestine but were barely detectable in gastric glands (Figure 5B and S10A). This positively correlated with MYC activity and suggests that EPCAM levels could be controlled by lysosomal degradation via endocytic or autophagic pathways. In agreement with this, MYC activation in CAG-Myc and CAG-Myc/Ctnnb1 mice led to marked EPCAM accumulation localized at the plasma membrane without altering CDH1 levels (Figure 5C and S10B-C). MYC-induced EPCAM stabilization was also confirmed in CAG-Myc and CAG-Myc/Ctnnb1 gastric organoids

(Figure 5D). Consistent with their central role in MYC-dependent suppression of lysosomal activity, the inhibition of mTOR and ERK in *CAG-Myc/Ctnnb1* gastric glands synergized in reducing EPCAM levels (Figure 5E). In line with this, MYC inhibition in intestinal organoids lowered mTOR and ERK activity and reduced EPCAM (Figure S10D). Indeed, treatment of WT gastric glands with three independent inhibitors of lysosome acidification (Chloroquine, Bafilomycin A1, and Ammonium Chloride) all increased EPCAM levels (Figure 5F). This effect was also confirmed in WT and *Ctnnb1*-derived gastric organoids by Chloroquine treatment (Figure 5G). To identify the specific pathways responsible for EPCAM degradation, we separately treated WT gastric glands with specific inhibitors of autophagy (SAR405), dynamin-dependent endocytosis (Dynasore), or macropinocytosis (EIPA), demonstrating a full macropinocytosis dependency (Figure 5F).

EPCAM is required for CTNNB1 chromatin localization and transcriptional activity

To determine whether EPCAM levels are directly involved in regulating CTNNB1 chromatin accumulation and WNT transcription, we silenced EPCAM expression in *CAG-Myc/Ctnnb1* organoids using two independent shRNAs. Upon EPCAM inhibition, regardless of exogenous Wnt3a stimulation, *CAG-Myc/Ctnnb1* organoids were reduced in size and lost their marked gland morphology, acquiring a cystic phenotype typical of low WNT activity (Figure 6A, 6B, S11A, and S11B). This correlated with a reduction in CTNNB1 chromatin occupancy (Figure 6C and 6D) and with the transcriptional silencing of both WNT-related and MycBcat tumor cluster marker genes (Figure 6E and S11C). Consistent with this, EPCAM silencing in *Ctnnb1* intestinal organoids compromised their growth (Figure 6F and S11D), reducing CTNNB1 chromatin occupancy (Figure 6G and S11E), which further correlated with WNT targets transcriptional silencing (Figure 6H). Indeed, CDH1 loss in *Ctnnb1* gastric organoids enhanced their formation efficiency, induced the acquisition of a gland-type morphology, and upregulated WNT markers similar to the *CAG-Myc/Ctnnb1* model (Figure 6I-K and S11F).

Together, this demonstrates that MYC-dependent regulation of EPCAM levels, suppressing its degradation by macropinocytosis, sustains WNT transcription, promoting CTNNB1 chromatin accumulation.

Regulation of EPCAM across the gastrointestinal tract is conserved in humans

To gain evidence that MYC controls lysosomal biogenesis and EPCAM levels in normal and pathological human contexts, we performed IF staining in gastric and colorectal cancer patients' sections containing parts of normal and tumor tissue. In the stomach, EPCAM levels were barely detectable in the normal tissue but were expressed at high levels in tumor areas (Figure 7A). This was different from the colon, which showed high EPCAM levels in both normal and tumor areas, in agreement with our mouse models (Figure 7A). Indeed, MYC expression was higher in the colon compared to the normal stomach tissue. Moreover, TFEB and TFE3 nuclear localization negatively correlated with MYC

expression and positively correlated with the levels of the lysosomal marker LAMP2 (Figure 7B and 7C). In line with this, MYC expression was increased in gastric tumors, accompanied by a reduction of TFE3 and TFEB nuclear localization and decreased LAMP2 levels (Figure 7B and 7D). This correlates with EPCAM accumulation, indicating a shared regulatory mechanism.

Journal Pre-proof

Discussion

Our results uncovered that WNT oncogenic mutations in *Lgr5*⁺ cells are not sufficient to induce tumors in the gastric epithelium compared to the small intestine. This agrees with previous studies showing that mutations of WNT pathway components, WNT ligands, as well as *H. pylori* infection or *Cdh1* mutations, are not sufficient to induce efficient gastric tumor formation^{2, 38-40}. Similarly, APCmin mice develop gastric tumors in elder life, suggesting an intrinsic constraint to WNT transformation and requirements of additional events⁴¹.

We have identified MYC levels as a limiting factor for WNT transcriptional activation and neoplastic transformation. This can be counterintuitive as *Myc* is considered a direct WNT target gene¹⁷. Our data suggest that MYC expression is independent from WNT signaling across gastrointestinal tissues. Indeed, MYC activity was shown to be essential for WNT-driven oncogenesis in the small intestine¹⁶, suggesting that WNT requires MYC to sustain its transcriptional programs but does not regulate its transcription. Low physiological MYC expression in *Lgr5*⁺ GC vs. IC could involve specific environmental signals, including Notch, SHH, JAK/STAT, ERK, and BMP/TGFB signaling⁴², to control the size of gastric glands, limiting the expansion of progenitors. The *Lgr5*⁺ GC and IC are characterized by distinct cell cycle speeds, and the nearly quiescent pace in the stomach^{2, 6} is directly linked to MYC-dependent negative regulation of lysosome biogenesis and autophagic catabolism.

Our results also indicate that MYC expression cooperates with CTNNB1 to enhance the activation of a WNT transcriptional program that triggers *Lgr5*⁺ GC proliferation, overwhelming the homeostatic potential of the isthmus region and expanding adenomas with stem-like properties and high WNT activity. This agrees with the efficient gastric tumor formation reported when WNT is activated together with proliferative signals like inflammation or P53/SMAD4 deletion³⁸⁻⁴⁰, which interestingly converge on MYC activation^{43, 44}. An interplay between MYC and CTNNB1 has also been observed in other tissues, including liver and blood, involving both cell and non-cell autonomous mechanisms⁴⁵⁻⁴⁷.

We demonstrate that MYC enhances WNT transcription, promoting CTNNB1 nuclear accumulation and chromatin invasion. Our results exclude a direct cooperation, linking CTNNB1 chromatin accumulation to MYC-dependent suppression of lysosomal biogenesis. This agrees with previous reports^{28, 30, 31} and points to MYC's negative competition with MiT/TFE²⁸. How MYC establishes transcriptional silencing still remains poorly understood, and competition with other activatory TFs (i.e., MIZ1) represents the most valuable model⁴⁸. Although this cannot be fully excluded, our data better support a mechanism that stimulates MiT/TFE cytoplasmic retention by MYC-dependent mTOR and ERK activation to enhance MYC-dependent metabolic rewiring.

We found that EPCAM levels are dampened by high lysosomal activity in the stomach specifically via macropinocytosis. CTNNB1 is also a component of adherent junctions where it binds to CDH1. This

interaction limits its transforming properties, acting as “a sink” for CTNNB1 oncogenic mutants⁴⁹. In this context, EPCAM was shown to sustain WNT signaling by destabilizing CDH1:CTNNB1 complexes at the plasma membrane^{36,37}. Low EPCAM expression in gastric glands and its stabilization upon MYC activation correlate well with CTNNB1 nuclear localization and chromatin association. Indeed, the specific requirement of EPCAM to sustain CTNNB1 chromatin invasion, WNT transcription, and a transformed phenotype corroborate this possibility.

We propose a model where MYC suppression of lysosomal biogenesis prevents macropinocytosis-dependent EPCAM degradation, raising its intracellular levels that prompt CTNNB1 chromatin accumulation. Importantly, we showed that this is conserved in humans at physiological and pathological levels, in agreement with EPCAM staining available in normal vs. gastric tumors from the Human Protein Atlas database (www.proteinatlas.org/ENSG00000119888-EPCAM). Overall, this provides a new mechanism that connects environmental signals and energy metabolism to gastric homeostasis and WNT-mediated transformation, which could be relevant also in more translational settings.

References

1. Ireland H, Kemp R, Houghton C, et al. Inducible Cre-mediated control of gene expression in the murine gastrointestinal tract: effect of loss of beta-catenin. *Gastroenterology* 2004;126:1236-46.
2. Barker N, Huch M, Kujala P, et al. Lgr5(+ve) stem cells drive self-renewal in the stomach and build long-lived gastric units in vitro. *Cell Stem Cell* 2010;6:25-36.
3. Barker N, van Es JH, Kuipers J, et al. Identification of stem cells in small intestine and colon by marker gene Lgr5. *Nature* 2007;449:1003-7.
4. Leushacke M, Tan SH, Wong A, et al. Lgr5-expressing chief cells drive epithelial regeneration and cancer in the oxyntic stomach. *Nat Cell Biol* 2017;19:774-786.
5. Leushacke M, Ng A, Galle J, et al. Lgr5(+) gastric stem cells divide symmetrically to effect epithelial homeostasis in the pylorus. *Cell Rep* 2013;5:349-56.
6. Tan SH, Swathi Y, Tan S, et al. AQP5 enriches for stem cells and cancer origins in the distal stomach. *Nature* 2020;578:437-443.
7. Sigal M, Logan CY, Kapalczynska M, et al. Stromal R-spondin orchestrates gastric epithelial stem cells and gland homeostasis. *Nature* 2017;548:451-455.
8. Wizenty J, Mullerke S, Kolesnichenko M, et al. Gastric stem cells promote inflammation and gland remodeling in response to *Helicobacter pylori* via Rspo3-Lgr4 axis. *EMBO J* 2022;41:e109996.
9. Nusse R, Clevers H. Wnt/beta-Catenin Signaling, Disease, and Emerging Therapeutic Modalities. *Cell* 2017;169:985-999.
10. Cancer Genome Atlas N. Comprehensive molecular characterization of human colon and rectal cancer. *Nature* 2012;487:330-7.
11. Cancer Genome Atlas Research N. Comprehensive molecular characterization of gastric adenocarcinoma. *Nature* 2014;513:202-9.
12. Morin PJ, Sparks AB, Korinek V, et al. Activation of beta-catenin-Tcf signaling in colon cancer by mutations in beta-catenin or APC. *Science* 1997;275:1787-90.
13. Harada N, Tamai Y, Ishikawa T, et al. Intestinal polyposis in mice with a dominant stable mutation of the beta-catenin gene. *EMBO J* 1999;18:5931-42.
14. Sansom OJ, Reed KR, Hayes AJ, et al. Loss of Apc in vivo immediately perturbs Wnt signaling, differentiation, and migration. *Genes Dev* 2004;18:1385-90.
15. He TC, Sparks AB, Rago C, et al. Identification of c-MYC as a target of the APC pathway. *Science* 1998;281:1509-12.
16. Sansom OJ, Meniel VS, Muncan V, et al. Myc deletion rescues Apc deficiency in the small intestine. *Nature* 2007;446:676-9.

17. Schaub FX, Dhankani V, Berger AC, et al. Pan-cancer Alterations of the MYC Oncogene and Its Proximal Network across the Cancer Genome Atlas. *Cell Syst* 2018;6:282-300 e2.
18. Dang CV. MYC, metabolism, cell growth, and tumorigenesis. *Cold Spring Harb Perspect Med* 2013;3.
19. de Souza CR, Leal MF, Calcagno DQ, et al. MYC deregulation in gastric cancer and its clinicopathological implications. *PLoS One* 2013;8:e64420.
20. Yeh CH, Bellon M, Nicot C. FBXW7: a critical tumor suppressor of human cancers. *Mol Cancer* 2018;17:115.
21. Mahe MM, Aihara E, Schumacher MA, et al. Establishment of Gastrointestinal Epithelial Organoids. *Curr Protoc Mouse Biol* 2013;3:217-40.
22. Onuma K, Ochiai M, Orihashi K, et al. Genetic reconstitution of tumorigenesis in primary intestinal cells. *Proc Natl Acad Sci U S A* 2013;110:11127-32.
23. Picelli S, Björklund AK, Reinius B, et al. Tn5 transposase and tagmentation procedures for massively scaled sequencing projects. *Genome Res* 2014;24:2033-40.
24. Chiacchiera F, Rossi A, Jammula S, et al. Polycomb Complex PRC1 Preserves Intestinal Stem Cell Identity by Sustaining Wnt/ β -Catenin Transcriptional Activity. *Cell Stem Cell* 2016;18:91-103.
25. Calado DP, Sasaki Y, Godinho SA, et al. The cell-cycle regulator c-Myc is essential for the formation and maintenance of germinal centers. *Nat Immunol* 2012;13:1092-100.
26. Soriano P. Generalized lacZ expression with the ROSA26 Cre reporter strain. *Nat Genet* 1999;21:70-1.
27. Bartfeld S, Bayram T, van de Wetering M, et al. In vitro expansion of human gastric epithelial stem cells and their responses to bacterial infection. *Gastroenterology* 2015;148:126-136.e6.
28. Annunziata I, van de Vlekkert D, Wolf E, et al. MYC competes with MiT/TFE in regulating lysosomal biogenesis and autophagy through an epigenetic rheostat. *Nat Commun* 2019;10:3623.
29. Garcia-Prat L, Kaufmann KB, Schneiter F, et al. TFEB-mediated endolysosomal activity controls human hematopoietic stem cell fate. *Cell Stem Cell* 2021;28:1838-1850 e10.
30. Yun S, Vincelette ND, Yu X, et al. TFEB links MYC signaling to epigenetic control of myeloid differentiation and acute myeloid leukemia. *Blood Cancer Discov* 2021;2:162-185.
31. Fernandez MR, Schaub FX, Yang C, et al. Disrupting the MYC-TFEB Circuit Impairs Amino Acid Homeostasis and Provokes Metabolic Anergy. *Cancer Res* 2022;82:1234-1250.
32. Medda A, Compagnoni M, Spini G, et al. c-MYC-dependent transcriptional inhibition of autophagy is implicated in cisplatin sensitivity in HPV-positive head and neck cancer. *Cell Death Dis* 2023;14:719.
33. Puissant A, Fenouille N, Auberger P. When autophagy meets cancer through p62/SQSTM1. *Am J Cancer Res* 2012;2:397-413.

34. Di Malta C, Cinque L, Settembre C. Transcriptional Regulation of Autophagy: Mechanisms and Diseases. *Front Cell Dev Biol* 2019;7:114.
35. Puertollano R, Ferguson SM, Brugarolas J, et al. The complex relationship between TFEB transcription factor phosphorylation and subcellular localization. *EMBO J* 2018;37.
36. Litvinov SV, Balzar M, Winter MJ, et al. Epithelial cell adhesion molecule (Ep-CAM) modulates cell-cell interactions mediated by classic cadherins. *J Cell Biol* 1997;139:1337-48.
37. Guerra E, Lattanzio R, La Sorda R, et al. mTrop1/Epcam knockout mice develop congenital tufting enteropathy through dysregulation of intestinal E-cadherin/beta-catenin. *PLoS One* 2012;7:e49302.
38. Oshima H, Matsunaga A, Fujimura T, et al. Carcinogenesis in mouse stomach by simultaneous activation of the Wnt signaling and prostaglandin E2 pathway. *Gastroenterology* 2006;131:1086-95.
39. Shimada S, Mimata A, Sekine M, et al. Synergistic tumour suppressor activity of E-cadherin and p53 in a conditional mouse model for metastatic diffuse-type gastric cancer. *Gut* 2012;61:344-53.
40. Park JW, Jang SH, Park DM, et al. Cooperativity of E-cadherin and Smad4 loss to promote diffuse-type gastric adenocarcinoma and metastasis. *Mol Cancer Res* 2014;12:1088-99.
41. Tomita H, Yamada Y, Oyama T, et al. Development of gastric tumors in Apc(Min/+) mice by the activation of the beta-catenin/Tcf signaling pathway. *Cancer Res* 2007;67:4079-87.
42. Kress TR, Sabo A, Amati B. MYC: connecting selective transcriptional control to global RNA production. *Nat Rev Cancer* 2015;15:593-607.
43. Warner BJ, Blain SW, Seoane J, et al. Myc downregulation by transforming growth factor beta required for activation of the p15(Ink4b) G(1) arrest pathway. *Mol Cell Biol* 1999;19:5913-22.
44. Santoro A, Vlachou T, Luzi L, et al. p53 Loss in Breast Cancer Leads to Myc Activation, Increased Cell Plasticity, and Expression of a Mitotic Signature with Prognostic Value. *Cell Rep* 2019;26:624-638 e8.
45. Kaveri D, Kastner P, Dembélé D, et al. β -Catenin activation synergizes with Pten loss and Myc overexpression in Notch-independent T-ALL. *Blood* 2013;122:694-704.
46. Ruiz de Galarreta M, Bresnahan E, Molina-Sánchez P, et al. β -Catenin Activation Promotes Immune Escape and Resistance to Anti-PD-1 Therapy in Hepatocellular Carcinoma. *Cancer Discov* 2019;9:1124-1141.
47. Bisso A, Filipuzzi M, Gamarra Figueroa GP, et al. Cooperation Between MYC and β -Catenin in Liver Tumorigenesis Requires Yap/Taz. *Hepatology* 2020;72:1430-1443.
48. Herkert B, Eilers M. Transcriptional repression: the dark side of myc. *Genes Cancer* 2010;1:580-6.
49. Huels DJ, Ridgway RA, Radulescu S, et al. E-cadherin can limit the transforming properties of activating beta-catenin mutations. *EMBO J* 2015;34:2321-33.

50. Nolte T, Brander-Weber P, Dangler C, et al. Nonproliferative and Proliferative Lesions of the Gastrointestinal Tract, Pancreas and Salivary Glands of the Rat and Mouse. *J Toxicol Pathol* 2016;29:1S-125S.
51. Kowalczyk MS, Tirosh I, Heckl D, et al. Single-cell RNA-seq reveals changes in cell cycle and differentiation programs upon aging of hematopoietic stem cells. *Genome Res* 2015;25:1860-72.

Journal Pre-proof

Figure 1: CTNNB1 and MYC cooperate to drive gastric cancer

- A)** H&E staining of gastric pyloric (stomach) and small intestinal (intestine) sections at 30 days PTI.
- B)** GFP expression in stomach and intestinal cryosections 30 days PTI. Nuclei were counter stained with DAPI.
- C)** FACS quantification of GFP⁺ cells of stomach and intestine 21 days PTI. *P* values were determined by non-parametric T-test.
- D)** RNA-seq tracks of *Myc* locus in *Lgr5*⁺ GC and IC from two independent *Lgr5*-GFP-CreERT2 WT mice (left). RT-qPCR analyses showing *Myc* expression in WT *Lgr5*⁺ GC and IC. *Tbp* served as normalization (right).
- E)** MYC staining in gastric and small intestinal cryosections derived from *Lgr5*-GFP-CreERT2 mice. Nuclei were counterstained with DAPI. Arrows indicate GFP⁺ cells (left). Violin-plots showing MYC fluorescence intensity quantifications (right). P-values were determined by non-parametric T-test. **** indicates a *P* value < .0001.
- F)** H&E staining (upper) and KI67 immunostaining (bottom) of gastric pyloric regions from indicated *Lgr5*-GFP-CreERT2 models 30 days PTI.
- G)** Histopathological score of gastric proliferative lesions as indicated according to Nolte et al.⁵⁰.
- H)** Representative images of B-galactosidase staining at day2 and day4 PTI (left). Percentage of LacZ⁺ cells in gland-base, isthmus or gland-base+isthmus at day2 PTI (middle) or during the time course (2, 4, 7, 14 days PTI) in the indicated mice (right).

Figure 2: CTNNB1 and MYC promote the expansion of undifferentiated *Lgr5*⁺ cells with high WNT activity

- A) IF staining for KI67 in gastric sections at 30 days PTI. GFP⁺ cells highlight *Lgr5*⁺ cells. Nuclei were counterstained with DAPI.
- B) FACS analysis quantification of *Lgr5* GFP⁺ cells from the gastric pyloric region of the indicated mice at 21 days PTI.
- C) IF analysis for GIF in gastric sections from the indicated mice at 30 days PTI (top). GFP⁺ cells highlight *Lgr5*⁺ cells. Nuclei were counterstained with DAPI. Alcian-Blue visualizes acid mucins (bottom).
- D) Volcano-plot showing RNA-seq DEGs of *Lgr5*⁺ GC derived from *CAG-Myc/Ctnnb1* mice vs. WT ($\text{Log}_2\text{FC} \geq 1$ vs. $-\text{Log}_{10} \text{P.adjust} \geq 2$) at 21 days PTI. Upregulated DEGs are shown in red, downregulated in green and non-significant genes in gray dots.
- E) GSEA of WNT and gastric cancer gene signatures of DEGs from D.
- F) scRNA-seq UMAP plot of epithelial (*Epcam*⁺) cells of the gastric pyloric regions of WT, *Ctnnb1*, *CAG-Myc* and *CAG-Myc/Ctnnb1* mice 30 days PTI. The plot shows common and sample-specific *Myc* (*CAG-Myc*) and *MycBeat* (*CAG-Myc/Ctnnb1*) clusters.
- G) UMAP plots showing the expression of the indicated genes in the *MycBeat* cluster.
- H) Expression Heatmap ($\text{Log}_2\text{-FC}$) for indicated gene signatures derived from scRNA-seq analyses. Cell cycle signature was obtained from Kowalczyk et al. ⁵¹.
- I) UMAP showing the median Z-score of the gene signature expression defined by the *CAG-Myc/Ctnnb1* upregulated proteins identified by LCM-MS analyses.
- J) IFITM3 IHC staining in the gastric pyloric region at 30 days PTI.
- K) Brightfield images of gastric organoids 6 days after replating in absence or in presence of Wnt3A where indicated.
- L) Heatmap ($\text{Log}_2 \text{FC}$) of RNA-seq analyses in organoids shown in K for the indicated gene signatures.

Figure 3: MYC enhances WNT transcriptional program increasing CTNNB1 chromatin accumulation

- A)** Heatmap of MYC ChIP-seq intensities over a ± 2.5 kb region from MYC peaks center ($-10\log_{10} p.adjust \geq 10$) in gastric organoids.
- B)** Overlap of MYC peaks detected in A.
- C)** As in A for CTNNB1 ChIP-seq.
- D)** Overlap of CTNNB1 peaks detected in C.
- E)** IHC staining for CTNNB1 in gastric pyloric sections at mice 30 days PTI.
- F)** Overlap between MYC and CTNNB1 peaks in *CAG-Myc/Ctnnb1* gastric organoids.
- G)** Distribution of MYC peaks between promoters ($\leq \pm 2.5$ kb from TSS) and distal regions ($> \pm 2.5$ kb from TSS).
- H)** As in G for CTNNB1 peaks.
- I)** Representation of the functional association to define MYC (blue) and CTNNB1 (green) target genes using promoter and distal sites.
- J)** Quantification of the expression difference (\log_2 FC) in *Lgr5+* GC (left) or in organoids (right) respective relative to WT and WT plus *Wnt3a* at MYC and CTNNB1 co-targets (MYC co-association) or for CTNNB1 unique targets (NO co-association).
- K)** Schematic mechanism for the enhanced activation of WNT transcriptional program upon MYC and CTNNB1 coactivation.

Figure 4: MYC suppresses lysosomal biogenesis and autophagy regulating MiT/TFE

- A)** Transcript per million (TPM) expression of genes belonging to the LYSOSOME (mmu04142) and AUTOPHAGY (GO:0006914) pathways in RNA-seq analysis of *Lgr5+* GC and IC.
- B)** Lyotracker Red mean fluorescence intensity (MFI) analyzed by flow cytometry in *Lgr5+* GC and IC. **** indicates a *P* value < .0001.
- C)** Quantification of LC3II/LC3I WB ratio of gastric pyloric glands and intestinal crypts from WT mice. **** indicates a *P* value < .0001.
- D)** As in B in *Lgr5+* GC from the indicated mice 21 days PTI. **** indicates a *P* value < .0001; ns = not significant.
- E)** Quantification of the expression difference (Log₂ FC) of genes belonging to the LYSOSOME and AUTOPHAGY pathways in the indicated gastric organoids relative to the WT+Wnt3a. **** indicates a *P* value < .0001; ns = not significant.
- F)** As in B in gastric organoids from the indicated mice.
- G)** As in C in gastric organoids from the indicated mice. *P* values: *** *P* < .001; **** *P* < .0001.
- H)** Percentage of deregulated lysosomal/autophagy related genes associated with a MYC ChIP-seq peak in *CAG-Myc/Ctnnb1* organoids ($\leq \pm 2.5$ kb TSS; top).
- I)** TFE3 and TFEB staining in gastric cryosections at 30 days PTI. Nuclei were counterstained with DAPI.
- J)** TFE3 and TFEB nuclear vs. cytoplasmic quantifications of the staining shown in I. **** indicates a *P* value < .0001.
- K)** As in B in *CAG-Myc/Ctnnb1* organoids after 24 hrs of 250 nM of Torin-1 (mTORi) and 2 μ M SCH772984 (ERKi) treatment. *P* values: *** *P* < .001; **** *P* < .0001.
- L)** WB of the indicated proteins in gastric organoids.
- M)** As in L in intestinal *Ctnnb1* organoids after treatment with 50 μ M of 10058-F4 (MYCi) for 24 hrs.
- N)** As in B in intestinal *Ctnnb1* organoids after treatment with 50 μ M of 10058-F4 (MYCi) for 24 hrs. **** indicates a *P* value < .0001

Figure 5: MYC promotes EPCAM stabilization suppressing macropinocytosis-dependent degradation

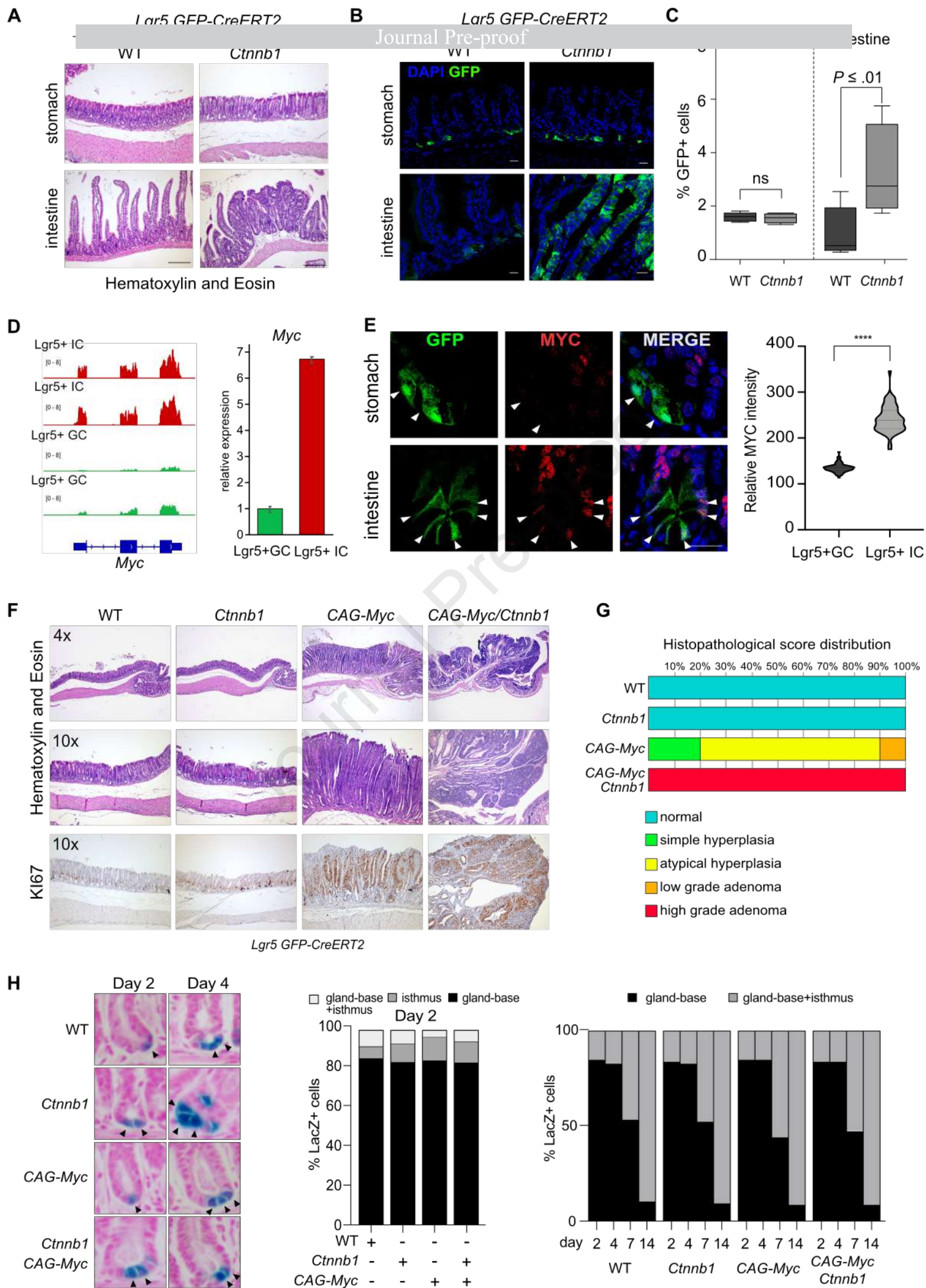
- A) Volcano-plot of differentially expressed proteins in *CAG-Myc/Ctnnb1* gastric epithelium.
- B) EPCAM staining of gastric and intestinal cryosections. GFP⁺ cells highlight Lgr5⁺ cells. Nuclei were counterstained with DAPI.
- C) As in B in gastric cryosections 30 days PTI.
- D) WB from gastric organoids at day 6 from replating. TUBULIN served as a loading control.
- E) EPCAM MFI analyzed by FACS in *CAG-Myc/Ctnnb1* gastric organoids 24 hrs from 250 nM Torin-1 (mTORi) or 2 μ M SCH772984 (ERKi) treatment.
- F) WB analysis of WT gastric glands upon SAR-405 (5 μ M), Dynasore (100 μ M), EIPA (50 μ M), Chloroquine (10 μ M), Bafilomycin A1 (25 nM), NH₄Cl (10 mM) treatments for 24 hrs. using the specified antibodies. TFR served as autophagy and endocytosis control while P62 and LC3 as autophagy-specific controls. Histone H3 was used for loading.
- G) WB analysis of WT and *Ctnnb1* gastric organoids treated with Chloroquine (10 μ M) for 24 hrs using the indicated antibodies.

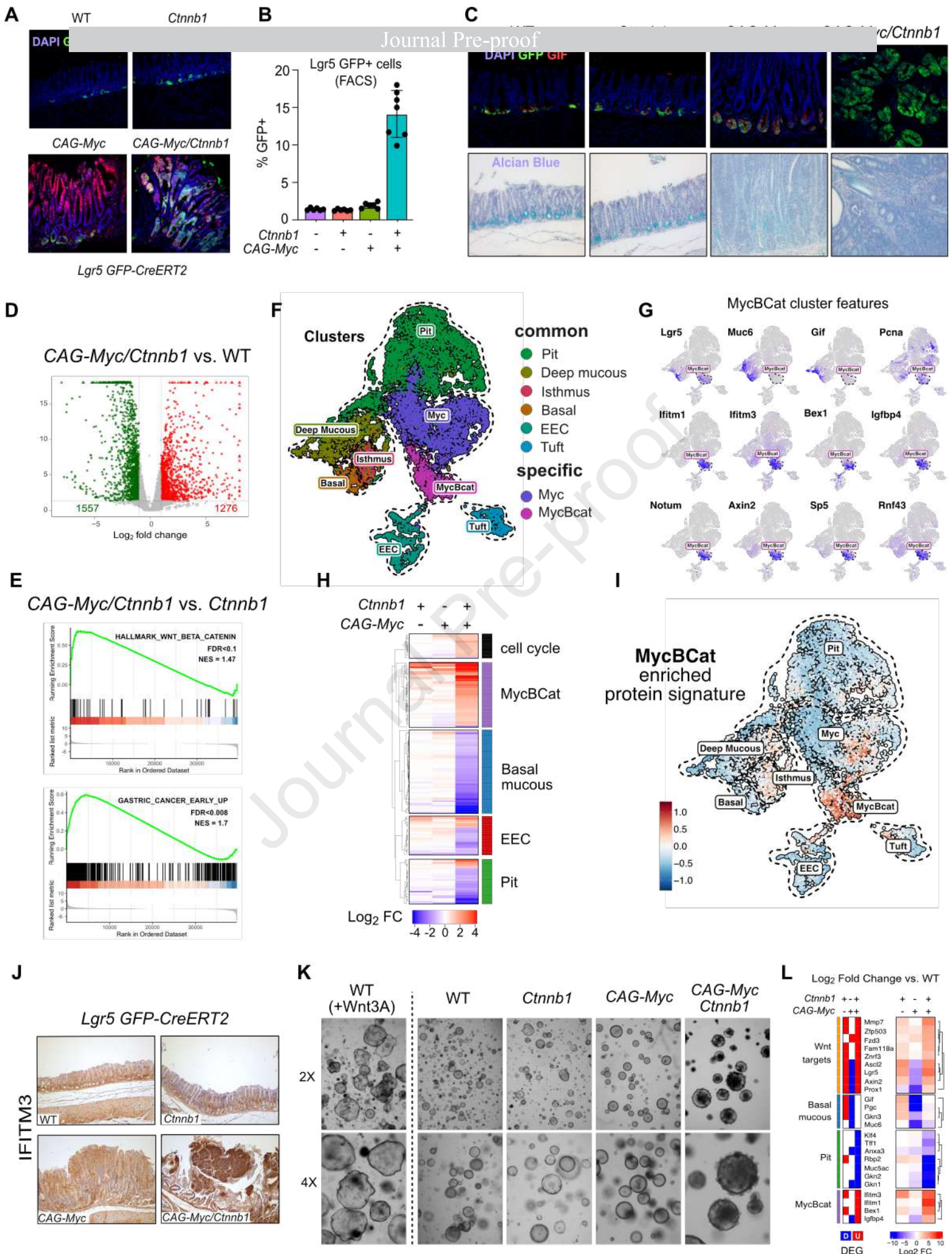
Figure 6: EPCAM sustains CTNNB1 chromatin accumulation and transcriptional activity

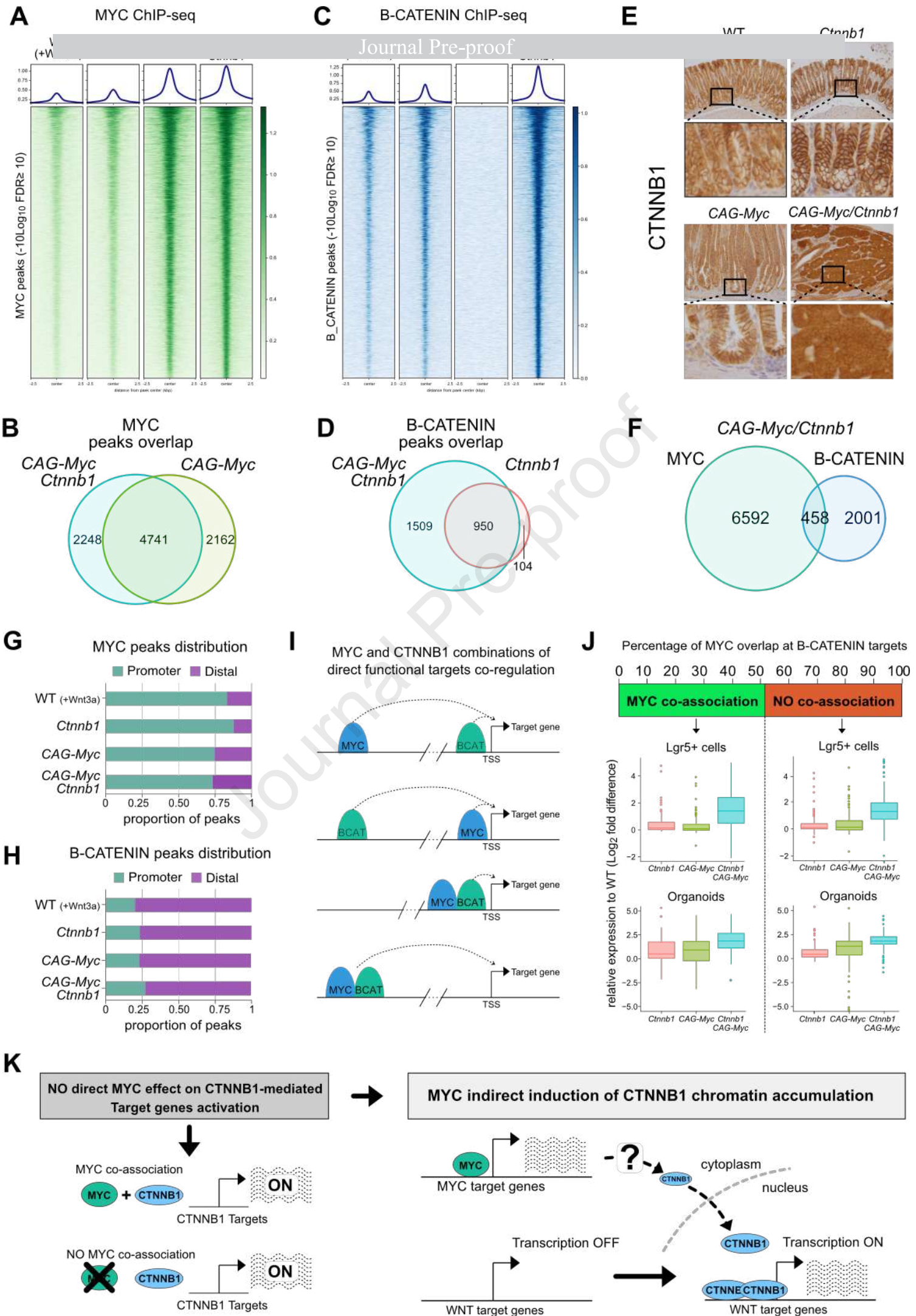
- A)** Bright field images of *CAG-Myc/Ctnnb1* gastric organoids transduced with lentiviruses expressing scramble (Ctrl) or two independent *Epcam* shRNAs sequences.
- B)** Quantification of morphology (left), size (middle) and formation efficiency (right) of *CAG-Myc/Ctnnb1* gastric organoids upon EPCAM interference. **** indicates a *P* value < .0001
- C)** Heatmap of CTNNB1 ChIP-seq intensities over a ± 2.5 kb region across peak center in *CAG-Myc/Ctnnb1* gastric organoids expressing the indicated shRNAs.
- D)** Quantification of CTNNB1 ChIP-seq intensities in *CAG-Myc/Ctnnb1* gastric organoids expressing the indicated shRNAs relative to WT gastric organoids of Figure 3C.
- E)** RT-qPCR expression analysis for the indicated genes in the organoids shown in A. *Thp* was used as normalizing control.
- F)** Bright field images of *Ctnnb1* intestinal organoids transduced with lentiviruses expressing scramble (Ctrl) or *Epcam* shRNA.
- G)** As in D for *Ctnnb1* intestinal organoids.
- H)** As in E for *Ctnnb1* intestinal organoids.
- I)** Bright field images of *Ctnnb1* gastric organoids expressing scramble (Ctrl) or *Cdh1* shRNA.
- J)** Morphology quantification of *Ctnnb1* gastric organoids from I.
- K)** As in E for the organoids shown in I.

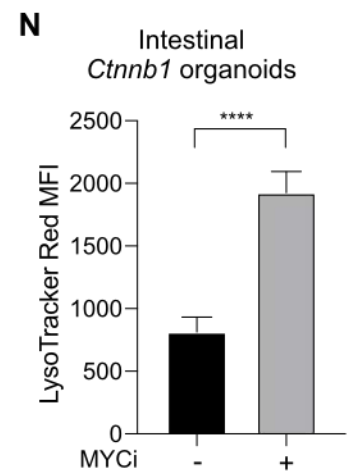
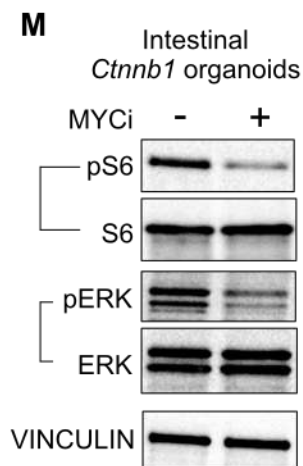
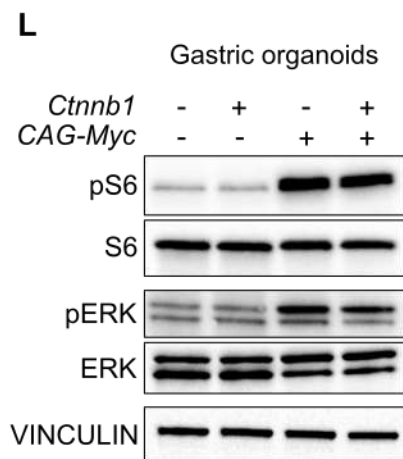
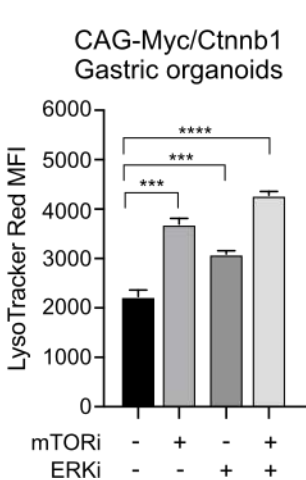
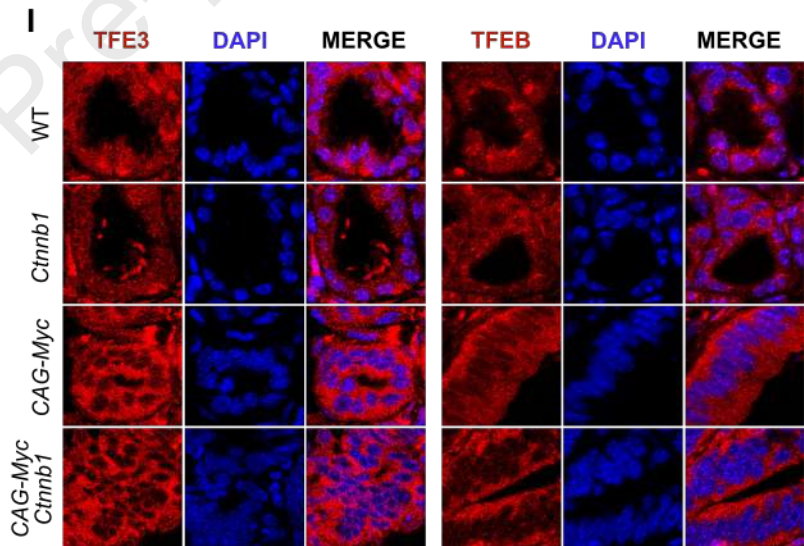
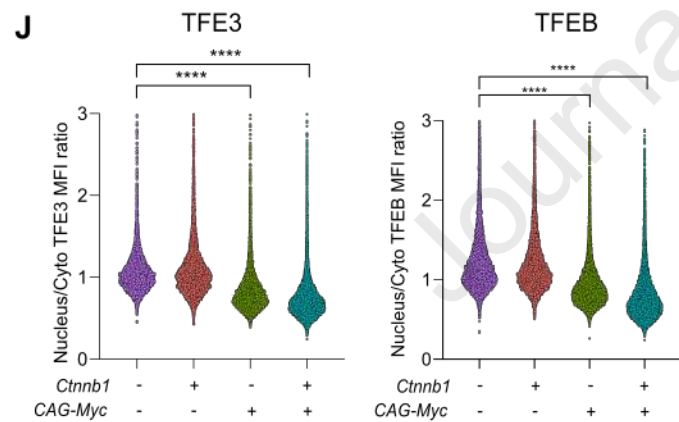
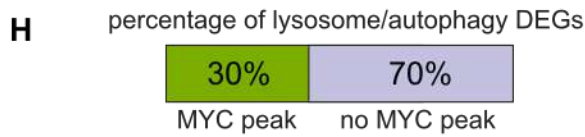
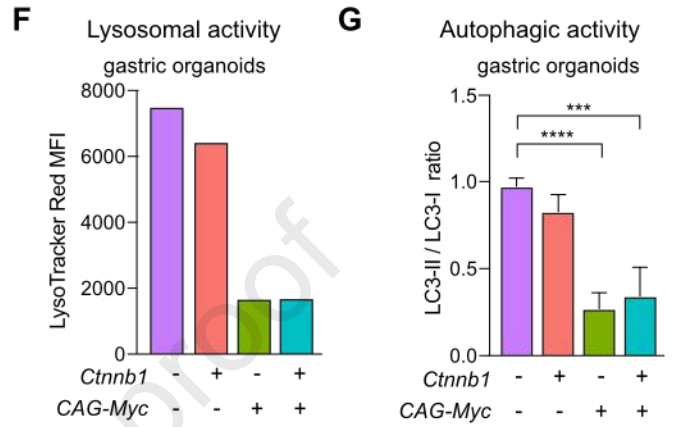
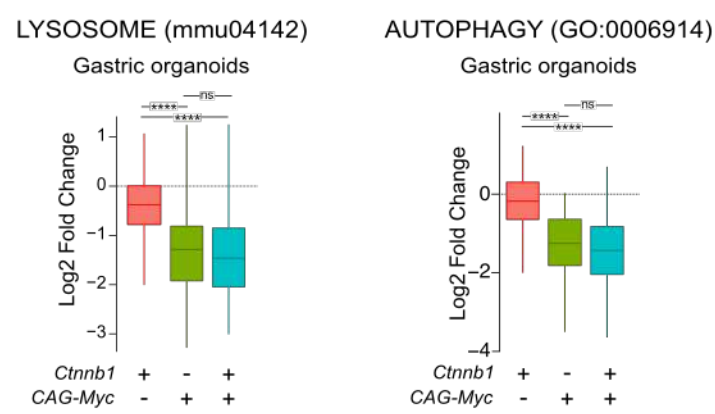
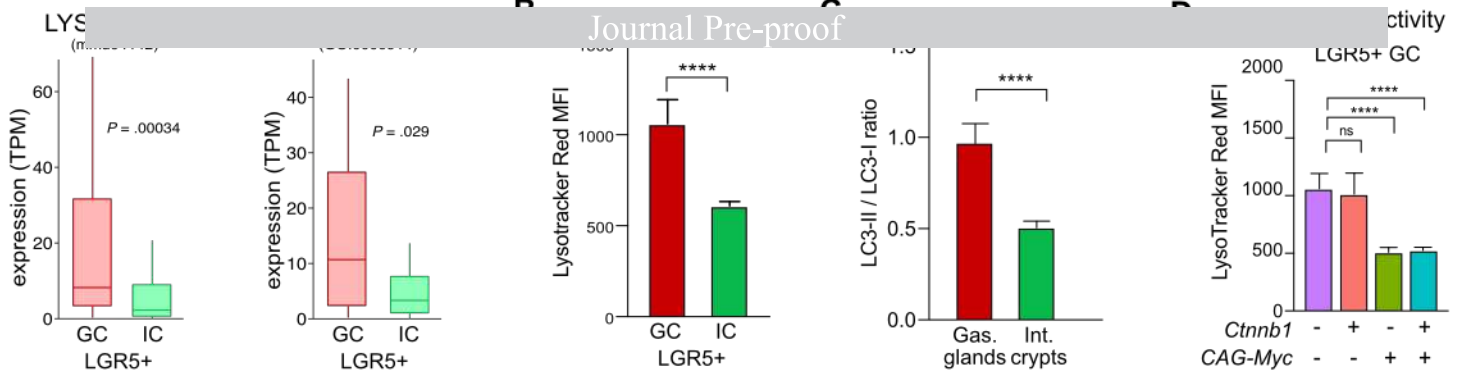
Figure 7: EpCAM regulation is preserved in human patient samples

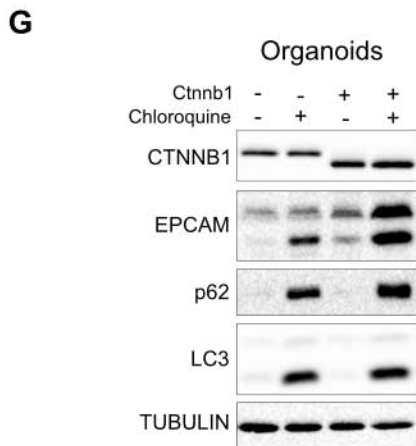
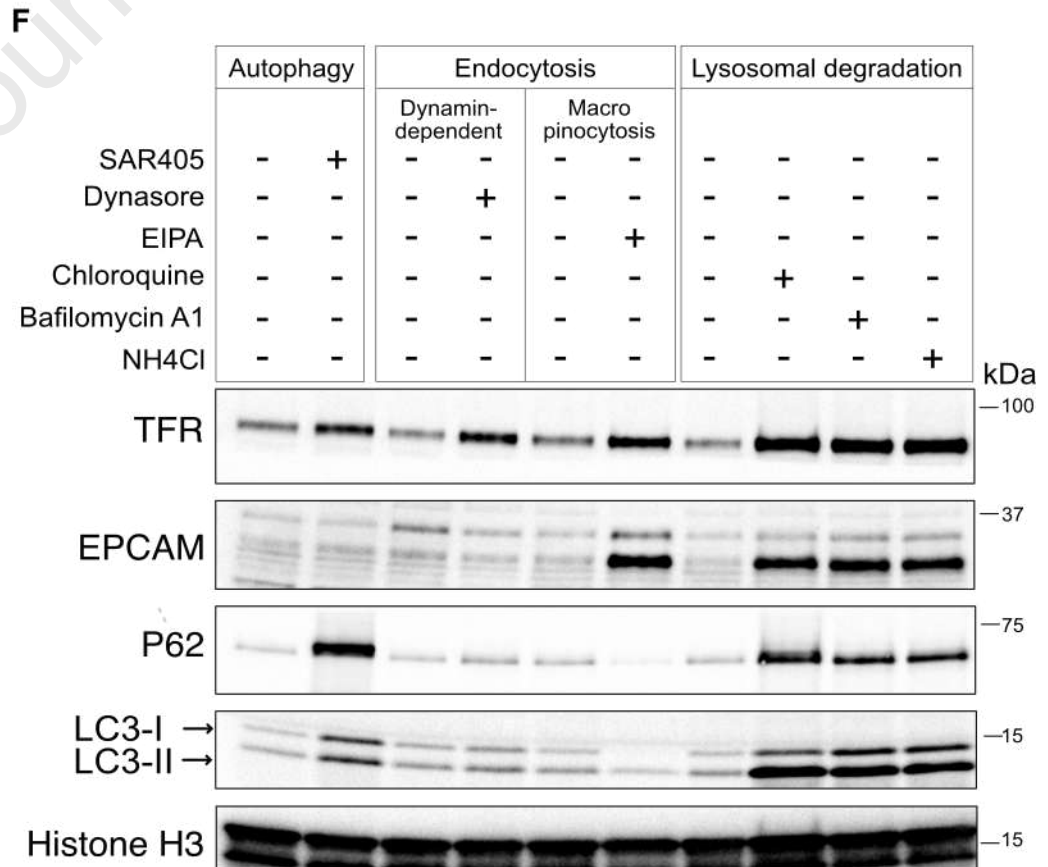
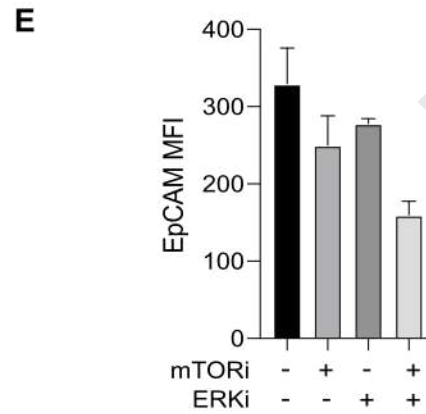
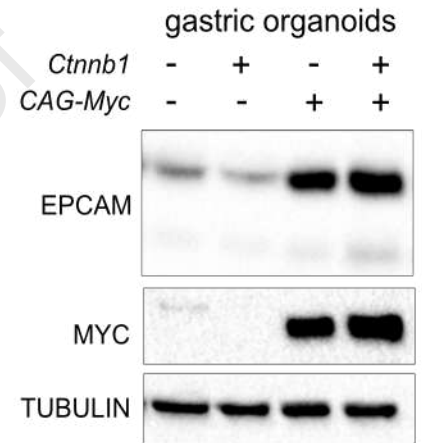
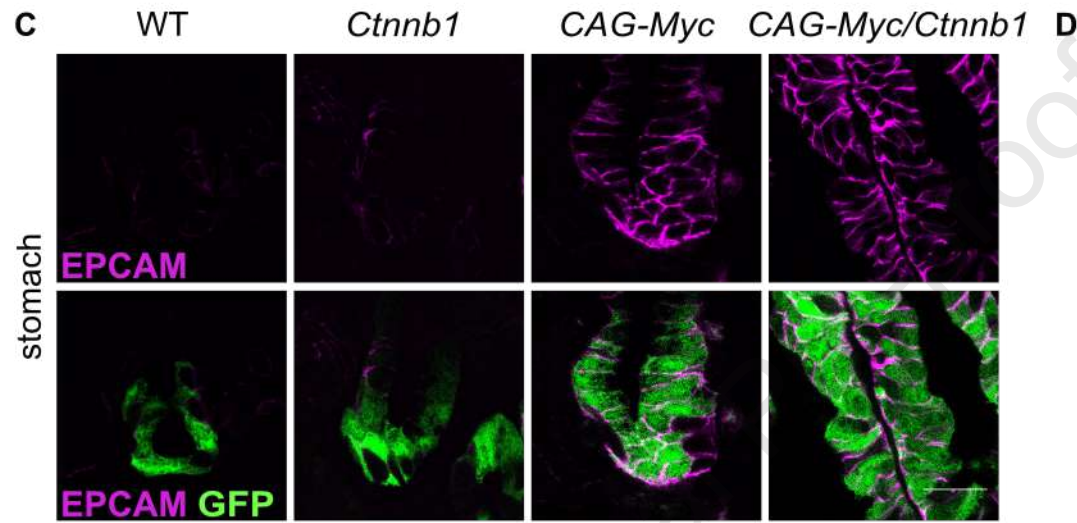
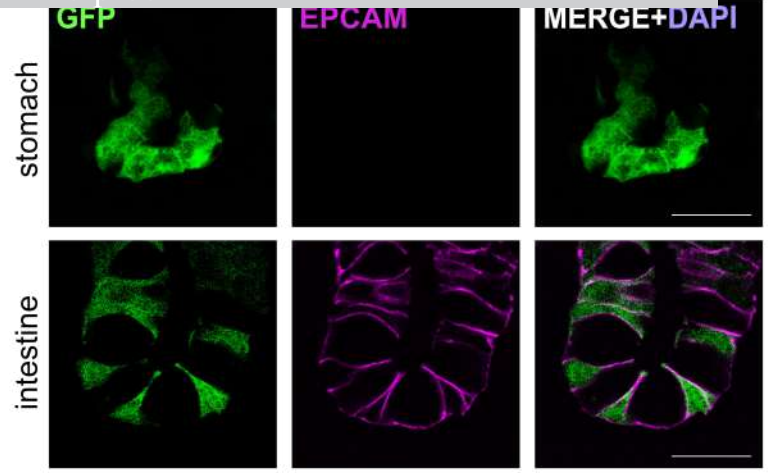
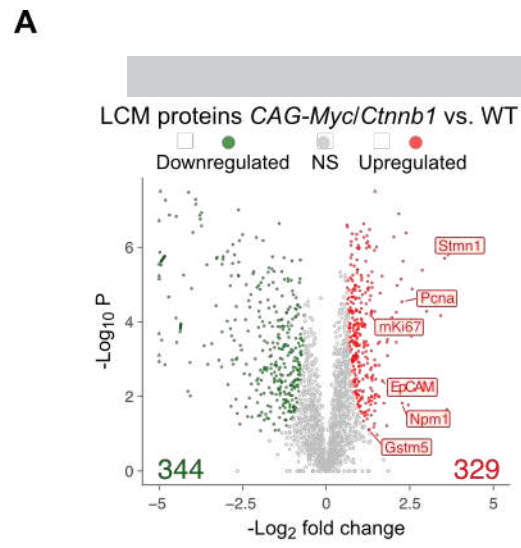
- A) EPCAM IF staining in gastric and colorectal patients' sections.
- B) IF stainings for the indicated markers in normal and tumour patient-derived gastric (left) and colorectal tissues (right).
- C) Quantification of fluorescence intensities for the indicated markers in gastric and colorectal normal human tissues. **** indicates a P value $< .0001$
- D) As in C in normal and tumour human gastric tissues. **** indicates a P value $< .0001$

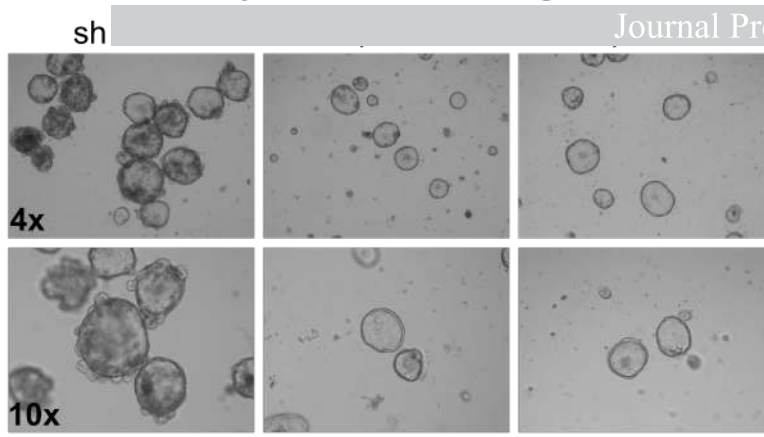
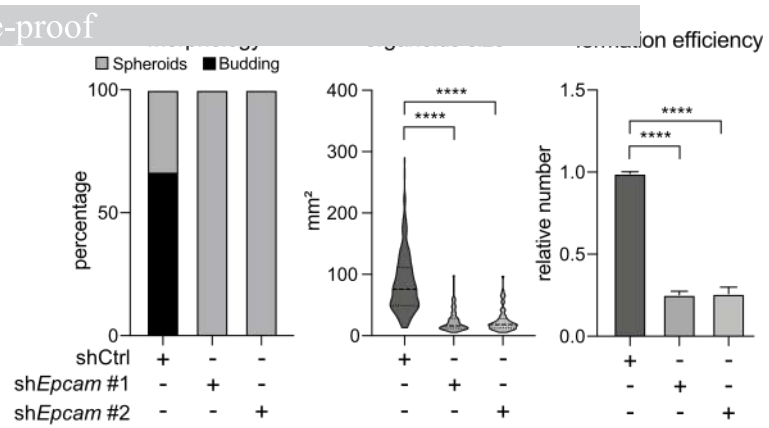
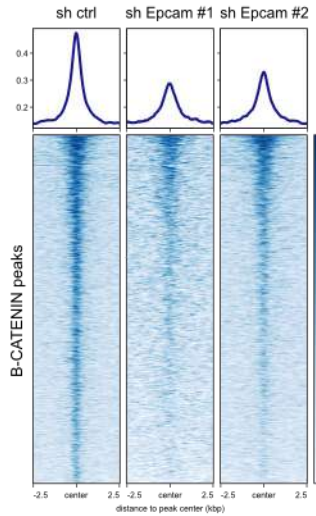
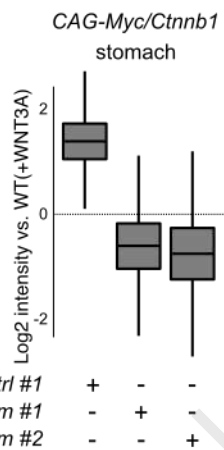
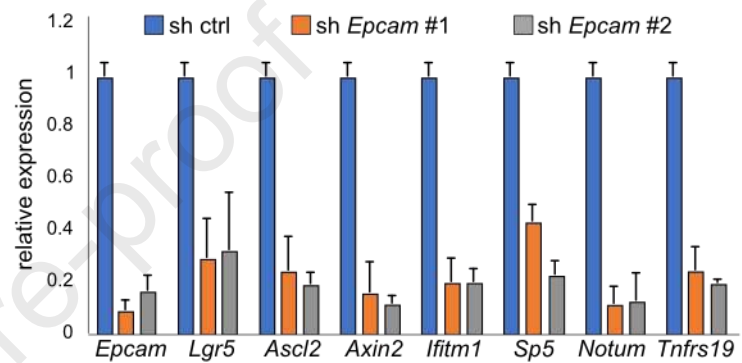
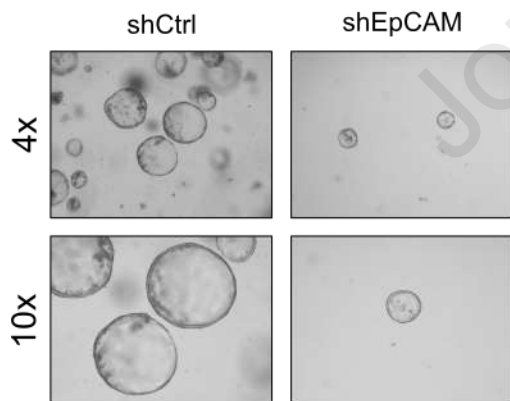
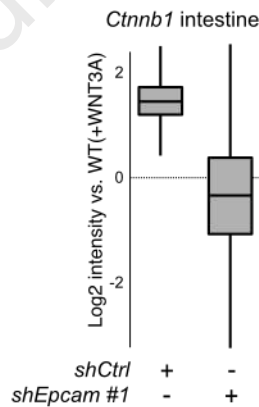
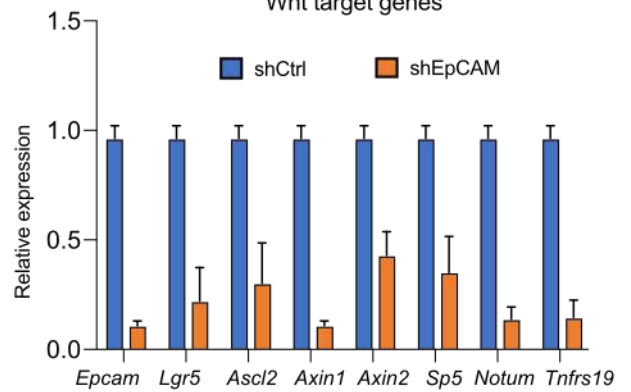
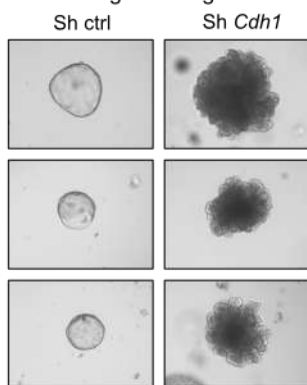
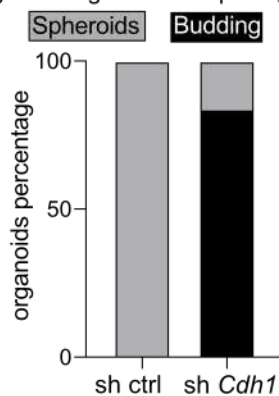
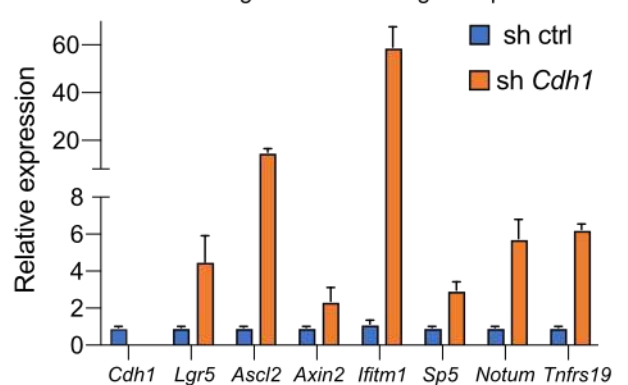










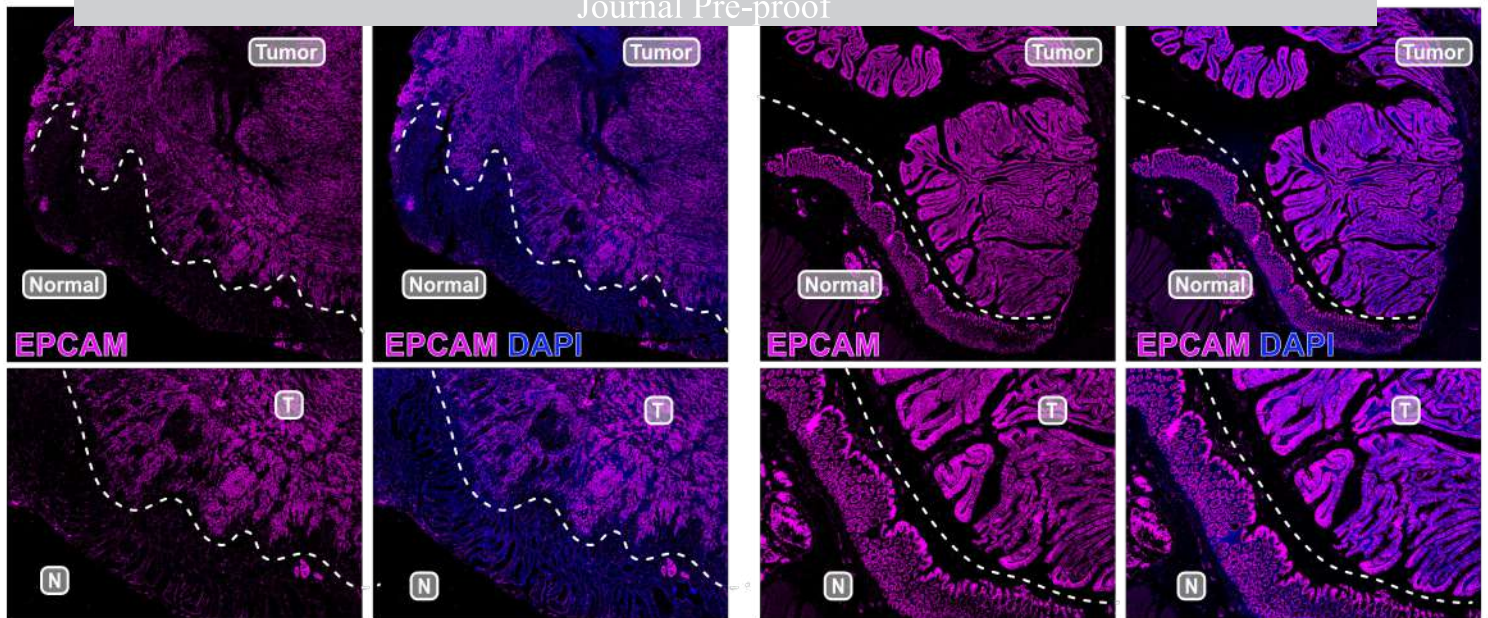
A**CAG-Myc/Ctnnb1 derived organoids****B****C****CAG-Myc/Ctnnb1 derived organoids****D****ChIP-seq B-CATENIN****E****CAG-Myc/Ctnnb1 derived organoids****F****Ctnnb1 derived intestinal organoids****G****ChIPseq B-CATENIN****H****Wnt target genes****I****Ctnnb1 gastric organoids****J****gastric organoids morphology****K****Ctnnb1 organoids -WNT targets expression**

A

Stomach

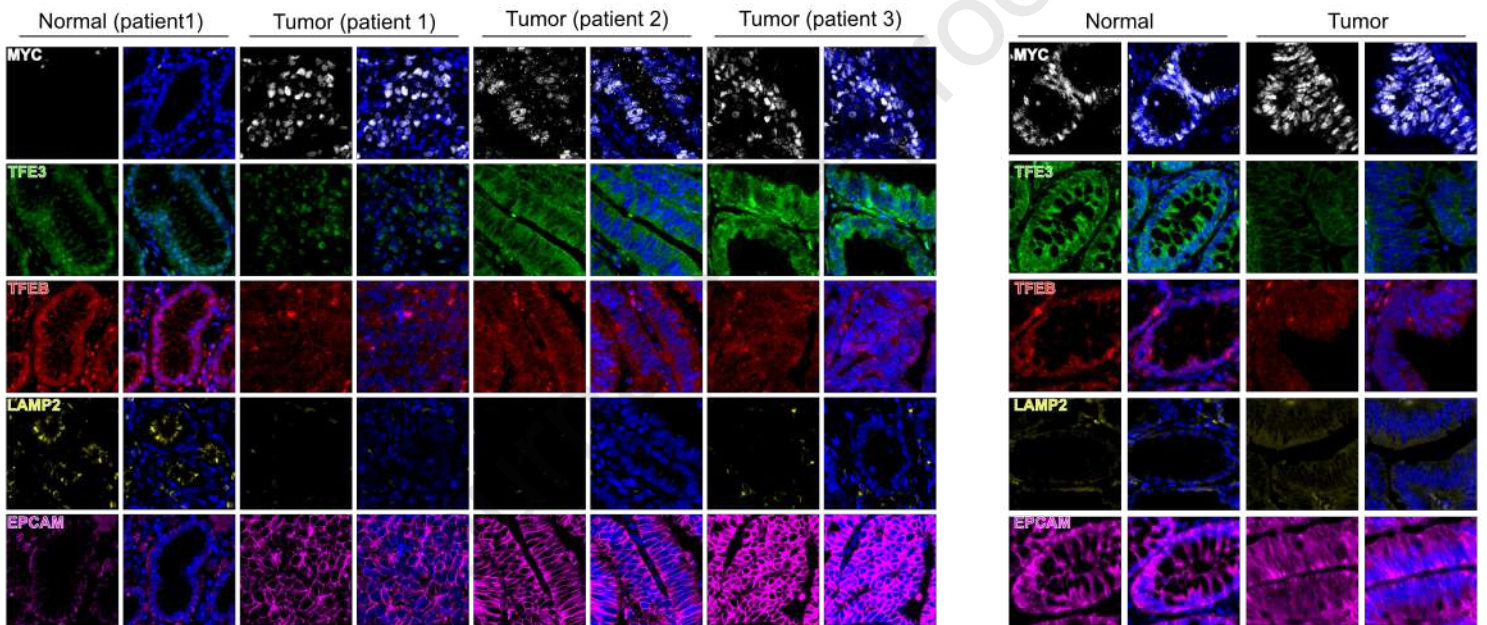
Colon

Journal Pre-proof

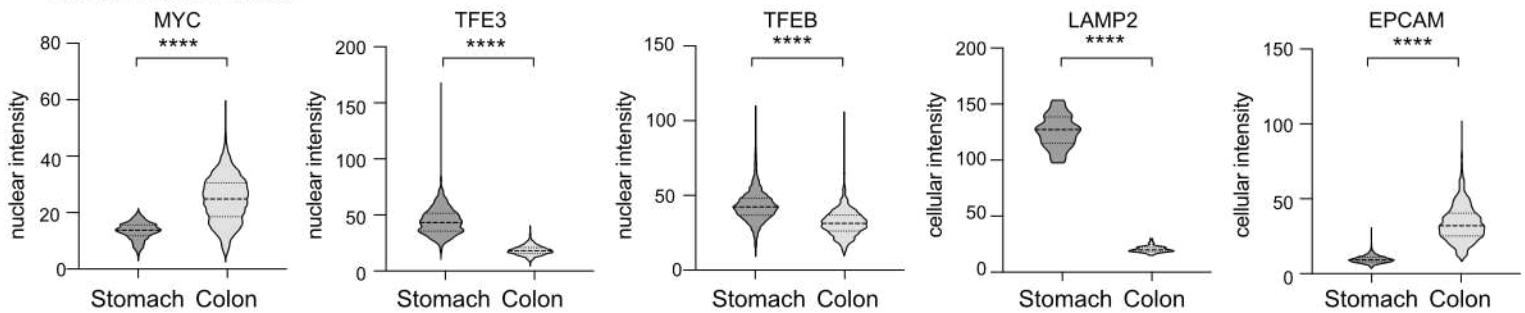
**B**

Human Stomach

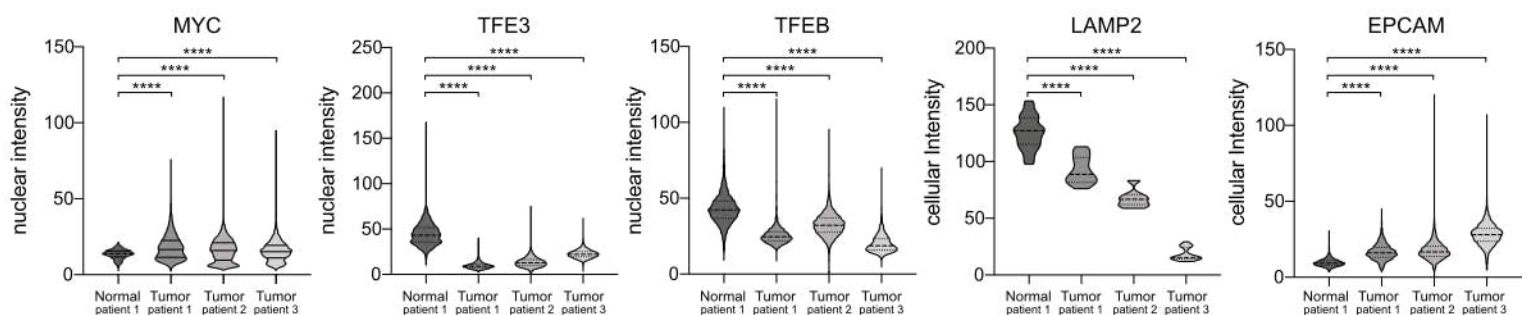
Human Colon

**C**

Human normal tissue

**D**

Human Stomach



What You Need to Know

Background and Context

WNT oncogenic mutations are common features of gastrointestinal tumors; however, their role in driving gastric carcinogenesis is poorly investigated at the molecular level.

New Findings

Oncogenic stabilization of B-CATENIN in the stomach is not sufficient to drive adenoma formation and requires MYC co-activation. MYC rewires cellular catabolic metabolism, suppressing both lysosomal biogenesis and autophagy, while activating mTOR and ERK signaling pathways. This reduces EPCAM degradative recycling by macropinocytosis favoring B-CATENIN nuclear accumulation to activate oncogenic WNT transcription programs.

Limitations

The model is specifically focused on Lgr5+ quiescent cells that control the gastric antrum homeostasis.

Basic Research Relevance

This study describes a new molecular mechanism by which high MYC activity is required to sustain the oncogenic properties of common WNT mutations across different gastrointestinal tracts conserved in mouse and humans.

Clinical Research Relevance

The mechanistic details uncovered by this study highlights new molecular vulnerabilities that could be exploited for therapeutic purposes by follow-up translational studies.

Lay Summary

WNT mutations are a hallmark of gastrointestinal cancer but low MYC activity represents a barrier for stomach adenoma formation. MYC regulates metabolic processes that allows WNT activation of oncogenic programs.

Supplementary material and methods

Animal Procedures

CTNNB1 stabilization was achieved using the *Ctnnb1*-ex3 conditional allele (here referred as *Ctnnb1*) which results in a Cre-dependent in frame deletion of *Ctnnb1* exon3¹. MYC overexpression was achieved using the Rosa26 *CAG loxP-STOP-loxP Myc* conditional allele² (here referred as *CAG-Myc*). In vivo lineage tracing was performed using the Rosa26 *loxP-STOP-loxP LacZ* conditional allele³. These alleles were crossed with the *Lgr5* GFP-CreERT2 transgenic model previously described in a C57BL/6 background⁴. Genotyping was confirmed by PCR of tail skin DNA using the primers listed in Table S6.

Histological analysis, Immunohistochemistry and Immunofluorescence

Stomach and small intestine were harvested at the indicated time points, opened longitudinally flushed with ice-cold PBS and fixed in 4% formaldehyde (FA) overnight at 4°C. The tissues were dehydrated in ethanol at increasing concentrations, immersed in Xylene and embedded in paraffin. The Formalin-Fixed Paraffin-Embedded (FFPE) samples were cut using microtome at 5 µm thickness.

For histological analysis, the sections were rehydrated and stained with Hematoxylin (Mayer Solution, Sigma Aldrich) for 2' at room temperature (RT). After three washes in water, cytoplasm were counter stained with Eosin Y (Sigma Aldrich). Sections were washed two times in ethanol 100%, immersed in Xylene and mounted with Eukitt (Bio-Optica). Images were acquired using Leica DM6 widefield microscope.

For immunohistochemistry, we performed heat-induced antigen unmasking using 10 mM sodium citrate followed by blocking in 5% donkey serum in 1X PBS for 1h at RT. Primary antibodies were incubated in blocking solution overnight at 4°C. Secondary antibody-HRP conjugated were incubated for 1h at RT and the signal was detected by using DAB substrate (Abcam 64238). Alcian-blue staining was performed following manufacturer's instructions (ThermoFisher 15432949).

For immunofluorescence, stomach and small intestine after isolation were fixed in 4% paraformaldehyde (PFA) for 2 hr at 4°C. Tissues were cryopreserved in 30% sucrose overnight and embedded in O.C.T. compound (Tissue-TEK 4583). OCT Embedded tissues were cut at 5 µm in thickness using cryostat. Sections were washed in tris-buffered saline-0.1% Tween 20 (TBS-T) and blocked with 5% donkey serum at RT for 1 hour. Sections were incubated with the primary antibodies overnight at 4 °C, washed in TBS-T, incubated for 1 hour at RT with secondary antibody and DAPI and finally mounted with Mowiol 4-88 (81381, Sigma-Aldrich). Images were captured using the SP8AOB confocal microscope (Leica Microsystems).

The primary antibodies used were as follows: Ki-67 (1:200; ab16667), CTNNB1 (1:200; Cell signaling 8480), c-MYC (1:200; Cell Signaling 9402), MUC5AC (1:200; Life Technologies MA512178), GIF

(1:500; kindly provided by D. Alpers), CHGA (1:200; Abcam ab84217), P62 (1:200; Abnova H00008878-M01), LC3 (1:200 Nanotools antibodies, 0231), TFE3 (1:200 HPA023881, Sigma-Aldrich), TFE3 (1:200; Bethyl Laboratories A303-673A), LAMP2 (1:200; Santa Cruz Biotechnology sc-18822), LAMP1 (1:1000, L1418 Sigma-Aldrich).

LacZ staining was performed as previously described⁵. Briefly, stomach was opened longitudinally, washed in PBS and fixed in ice-cold glutaraldehyde/PFA for 2 hr at 4°C. β -Galactosidase staining was performed overnight at RT. Then, tissues were washed in PBS, fixed in 4% PFA for 6 hrs and paraffin embedded.

Laser Capture Microdissection and Mass spectrometry analysis

FFPE sections were deparaffinized with xylene and then rehydrated in an ethanol gradient up to 75% Ethanol. Sections were stained with Cresyl Violet solution (0.8% Cresyl Violet in 60% EtOH and 4 mM Tris-HCl, pH 8.0) for 1 minute to visualize histological structures. Then, they were washed two times in 75% ethanol and air dried. Regions of 3000 cells per sample were cut using a UV-based LMD7 laser microdissection system (Leica Microsystems) at 20x magnification. Micro-dissected areas were collected by gravity into strip-tube caps and kept dry at 4°C until further processing.

For mass spectrometry analysis, LCM samples were digested using the PreOmics iST preparation kit, following the manufacturer's instructions. Whole section tissues were also digested in parallel to generate a reference library using the PreOmics iST kit and fractionated through the Pierce™ High pH Reversed-Phase Peptide Fractionation Kit (Thermo Fisher Scientific), obtaining 8 fractions. In all cases, peptide mixtures were separated by reversed-phase chromatography on an EASY-nLC 1200 ultra-high-performance liquid chromatography (UHPLC) system through an EASY-Spray column (Thermo Fisher Scientific), 25-cm long (inner diameter 75 μ m, PepMap C18, 2 μ m particles), which was connected to a Q Exactive HF (Thermo Fisher Scientific) instrument through an EASY-Spray™ Ion Source (Thermo Fisher Scientific). Purified peptides were loaded in buffer A (0.1% formic acid in water) at constant pressure of 980 Bar and separated with the following gradient scheme: 84 min of 3-30% of buffer B (0.1% formic acid, 80% acetonitrile), 5 min 30-60% of buffer B, 1 min 60-95% buffer B, at a constant flow rate of 300 nl/min. The column temperature was kept at 45°C under EASY-Spray oven control. For the library samples, the mass spectrometer was operated in data-dependent acquisition (DDA) mode (Top-15). MS spectra were collected in the Orbitrap mass analyzer at a 60,000 resolution (200 m/z) within a range of 300–1650 m/z with an automatic gain control (AGC) target of 3e6 and a maximum ion injection time of 20 ms. The 15 most intense ions from the full scan were sequentially fragmented with an isolation width of 1.4 m/z, following higher-energy collisional dissociation (HCD) with a normalized collision energy (NCE) of 28%. The resolution used for MS/MS spectra collection in the Orbitrap was 15,000 at 200 m/z with an AGC target of 1e5 and a maximum ion injection time of 80 ms. Precursor dynamic exclusion was enabled with a duration value of 20s. The LCM samples were

analyzed using BoxCar acquisition mode ⁶ and the mass spectrometer was operated under MaxQuant. Live control, with default parameters ⁷. MS Raw files were processed with MaxQuant version 1.6.0.15, and the extracted MS/MS spectra were matched by the Andromeda search engine against tryptic peptides (maximum of two missed cleavages) derived from mouse reference proteomes (Uniprot UP000000589, 55331 entries). The search included cysteine carbamidomethylation as a fixed modification and methionine oxidation and acetylation of the protein N-terminus as variable modifications. Required minimum peptide length was seven amino acids and maximum mass tolerances were 4.5 p.p.m. for precursor ions after nonlinear recalibration and 20 p.p.m. for fragment ions. MaxLFQ as performed separately in parameter groups with a minimum ratio count of 1. If applicable, peptide identifications were transferred between samples by match-between-runs (MBR) function using a 0.7 min window after retention time alignment. Identifications in the library were filtered for a FDR < 1% at both at peptide and protein levels ⁸. The protein-groups output table from MaxQuant was analysed using the Perseus software ⁹ to remove “reverse”, “only identified by site”, “contaminants”, and at least 70% data completeness in each group. Data were not imputed and to determine significantly changing proteins, a two-sample Student's t-test was used.

Intestinal crypts and stomach glands isolation

Isolated small intestine was flushed with ice-cold PBS and opened longitudinally. Villi were scraped using glass coverslips, the tissue was cut into small pieces and incubated in 5 mM EDTA in PBS for 45 minutes on a rotating wheel at 4°C. Tissue fragments were shaken roughly and the suspension was filtered using a 70 µm cell strainer (BD Bioscience) to isolate intestinal crypts.

For gastric pyloric gland isolation, the stomach was opened longitudinally and washed with ice-cold PBS. Pyloric region was selected and the serosal muscle was stripped using fine-point curved forceps under the dissector stereomicroscope (Leica M 205A). The gastric pyloric region was cut into small pieces and incubated in 10 mM EDTA in PBS on a rotating wheel for 2 hours at 4°C. Supernatant was removed and stomach fragments were re-suspended in dissociation buffer (43.4 mM sucrose, 54.9 mM D-sorbitol in PBS). The tissues were shaken vigorously to dissociate individual glands and the suspension was filtered using 100 µm cell strainer to isolate gastric glands.

For single cell dissociation, intestinal crypts or gastric glands were incubated in a solution composed by Tryple Express (Gibco), DNase I (Roche) 2000 U/ml, 10 nM ROCK inhibitor Y-27632 (Selleckem) for 15 minutes at 37 °C. Tryple Express was inactivated with FBS and falcon was shaken roughly to efficiently separate the single cells. Dissociated cells were filtered with a 40 µm cell strainer and resuspended in PBS for further analysis.

Flow cytometric analysis and sorting of *Lgr5*+ cells

For Lysotracker staining, single intestinal and gastric pyloric cells were incubated for 20 min with 80

nM of LysoTracker Red (HY-D1300, MedchemExpress). Then, the cells were washed, resuspended in PBS and analyzed using the BD FACS Celesta. For EPCAM staining, single cells were blocked in 5% BSA in PBS for 1 hr and stained with 1 μ g of EPCAM antibody in BSA 1% in PBS (Thermo Fisher 48-5791-82) for 1 hr. After the incubation, cells were washed twice in PBS and acquired using the BD FACS Celesta.

For *Lgr5*⁺ cells sorting, single cell suspensions from small intestine and gastric pyloric regions were resuspended in Sorting Medium composed by Advanced Dulbecco Modified Eagle Medium (ADMEM)/F12 (Invitrogen) supplemented with 10 mM HEPES, 2mM Glutamine (Lonza), 100 U/ml penicillin and 0.1 mg/ml streptomycin, 1.25 mM N-acetyl-cysteine (Sigma-Aldrich), N2 (Invitrogen), B27 (Invitrogen). These suspensions were filtered with 40 μ m cell strainer to eliminate cell aggregates. To discriminate between live and dead cells, we added Propidium Iodide (PI) at a final concentration of 25 μ g/ml. We sorted GFP⁺ve PI⁻ve GSCs and ISCs using FACS Melody sorter (BD Biosciences). The quantification of FACS data was carried out using the FLOW JO software.

Organoids culture

Gastric pyloric or intestinal single cells were embedded in Matrigel (BD Biosciences), plated on 24-well plates and incubated at 37°C for 20 min to allow the Matrigel polymerization. Organoids were cultured in Advanced DMEM/F12, supplemented 10 mM HEPES, 2mM Glutamine (Lonza), 100 U/ml penicillin and 0.1 mg/ml streptomycin, 1.25 mM N-acetyl-cysteine (Sigma-Aldrich), N2 (Invitrogen), B27 (Invitrogen). This basal medium was supplemented with 50 ng/ml EGF (Healthcare), 100 ng/ml Noggin (Preprotech), 10 μ M Y-27632 (Selleck Chemicals) and 10 μ M Jagged-1 (MedchemExpress) for the intestinal organoids and further supplemented with Human 100 ng/ml FGF-10 (Preprotech) 10 nM Human Gastrin I (Sigma) for the gastric organoids culture. WT organoids were cultured in presence of 10% R-spondin1 conditioned medium (homemade) and when indicated in the presence of 20% recombinant Wnt3a conditioned medium (homemade). The medium was replaced every 2 days.

For lentiviral infections, single cells were transduced with concentrated lentiviral particles and seeded on top of polymerized Matrigel in a 48 well plate as previously described¹⁰. Transduction was carried out over-night and the following morning the medium was changed. Transduced cells were selected in Puromycin (2 μ g/ml) for 72 hours. shRNAs sequences cloned in a pLKO.1 lentiviral vector (Sigma-Aldrich) are reported in Table S6.

Drugs Treatments

When indicated, glands and organoids were treated with Chloroquine (Sigma, 10 μ M), Bafilomycin A1 (Sigma-Aldrich, 25 nM), NH₄Cl (Sigma-Aldrich, 10 mM), SAR405 (MedChemExpress, 5 μ M), Dynasore (Sigma-Aldrich, 100 μ M), EIPA (Sigma, 50 μ M), SCH772984 (Selleckchem, 2 μ M),

TORIN-1 (Selleckchem, 250 nM), CHIR-99021 (Selleckchem, 5 μ M), LY294002 (MedChemExpress, 10 μ M), 10058-F4 (Sigma-Aldrich, 50 μ M) for 24 hrs.

Protein extraction and Western Blot

Intestinal crypts, gastric glands and organoids were lysed with S300 extraction buffer (20 mM Tris-HCl pH 8, 300 mM NaCl, 10% Glycerol, 0.2% Igepal) with protease inhibitor cocktail (Roche P8340) for 20 minutes on ice, sonicated for 10 cycles at 30' using Bioruptor sonicator. The cell debris were removed by centrifugation at 13000 rpm for 20 minutes at 4° C. Protein concentration was determined using a BIO-RAD Protein Assay. Western blots were performed using anti-MYC (Cell Signaling 9402), anti-EpCAM (abcam ab71916), anti-ECADHERIN (Cell signaling 3195), anti-P62 (Abnova H00008878-M01), anti-LC3 (Sigma L7543), anti-CTNNB1 (Cell signaling 8480), anti-pS6 (Cell Signaling 2211), anti-S6 (Cell Signaling 2217), anti-pERK1/2 (Cell Signaling 9101), anti-ERK1/2 (Cell Signaling 9102) anti-TUBULIN (Cell signaling 2144) anti-VINCULIN (Santa Cruz Biotechnology SC-73614), anti-ACTIN (Sigma A3853), anti-H3 histone (Abcam ab1791) antibodies.

RNA extraction and Real time Quantitative PCR (RT-qPCR)

RNA extraction was performed lysing the cells with Quick-RNA MiniPrep kit (Zymo Research) following manufacturer instructions. Purified RNA was quantified at NanoDrop. RNA was retrotranscribed using the ImProm-II™ Reverse Transcriptase reagents, following the Promega standard protocol. Retrotranscribed cDNA was analyzed by RT-qPCR with GoTaq qPCR Master Mix following manufacturer instructions (Promega).

Single cell RNA-seq

Stomachs were opened longitudinally, washed with ice-cold PBS and gastric pyloric regions were selected under the dissecting stereomicroscope. The gastric pyloric regions were incubated with a solution containing Collagenase IV (Sigma) and Dispase II (Sigma) enzymes at 37°C for 20 minutes, washes two times in PBS and incubated with 2 mM EDTA in PBS on a rotating wheel at 4°C for one hour. Supernatant was removed and tissues fragments were re-suspended in dissociation buffer (43.4 mM sucrose, 54.9 mM D-sorbitol in PBS). The tissue pieces were shaken vigorously to dissociate individual glands from tissue and were collected by passing through a 100 μ m cell strainer. Medium containing dissociated glands was centrifuged at 1200 rpm for 5 minutes and incubated with Tryple Express (Gibco), DNase I (Roche) 2000 U/ml, 10 nM ROCK inhibitor Y-27632 (Selleckem) for 15 minutes at 37 °C. Dissociated single cells were extensively washed in 1XPBS, filtered with a 40 μ m cell strainer and resuspended in sorting medium. Propidium Iodide (PI) was added to a final concentration of 25 μ g/ml and isolated PI- single gastric pyloric cells on a FACS Melody sorter (BD Biosciences). Sorted cells were counted and used to perform single cell RNA-seq analysis following the 10x Genomics Chromium Single Cell Gene Expression Flex instructions and sequenced on Illumina Novaseq 6000. Briefly, demultiplexing, assignment of barcodes and quantification of UMIs was

performed with cellranger using default parameters. Reads were aligned to the reference genome mm10, already pre-built by 10XGenomics (<http://software.10xgenomics.com/single-cell/overview/welcome>). Cells with less than 500 UMI, 200 detected genes and more than 30% of UMIs corresponding to mitochondrial reads were removed in order to keep only high-quality cells. Further downstream analyses were performed using Seurat (v3) ¹¹ pipeline based on the function SCTransform ¹². The Pearson residuals of the top 3000 most variable genes were used to calculate the first 15 principal components, which were used as input for the function FindNeighbors, together with a k.param of 25. Clusters were determined with the function FindClusters with a resolution parameter of 0.2. Clusters were manually curated and annotated based on markers available in the literature. Marker genes for each cluster were defined with the function FindAllMarkers with parameters *min.pct=25* and *test.use=wilcox*.

Bulk RNA sequencing

Cells were lysed in a buffer containing Tryton X-100 0,2%, RNase inhibitor 4 U/μL. The samples were incubated for 3 minutes at 72°C with 1 μL of 10 mM oligo-dT30Vn and 1 μL of 10 mM DNTPs to allow RNA unfolding and oligo annealing with the polyA end of messenger-RNA. Samples were retro transcribed using a mix containing SuperScript III RT enzyme 100U/μL (Invitrogen), RNase Inhibitor 10U/μL, Betaine 1M, DTT 5 mM, MgCl₂ 6mM and TSO 1 μM (Template Switching Oligo). Retro transcription reaction was performed following the manufacturer instructions. Samples were pre-amplified using High Fidelity KAPA taq HotStart kit. Reactions were purified with AMPure XP beads (Agencourt AMPure XP, Beckman Coulter). Purified cDNA quality was assessed using Bioanalyzer instrument (Invitrogen).

NGS Libraries were prepared using Tn5 based tagmentation reaction. Briefly, 2ng of cDNA was tagmented with 100 ng of Tn5 enzyme (homemade) pre-annealed with A/B-MEDS (Mosaic End Double-Stranded) oligonucleotides in a working buffer containing TAPS-NaOH pH 8.5 5mM, PEG 8000 8% for 5 minutes at 55°C. The tagmented DNA fragments were purified with AMPure beads and amplified using High fidelity KAPA Taq HotStart kit with the addition of 2 μM Ad1 Primer (i5 primer for Illumina sequencing Without Barcode) and 2μM Ad2.X Primer (i7 primer for Illumina sequencing containing different Barcodes). The resulting libraries were purified, quantified and sequenced using NovaSeq 6000.

Paired-end reads were aligned using STAR v2.7 to mm10 with default parameters plus –outFilterMultimapNmax 1 to block reads multimapping. PCR duplicates were removed using samblaster ¹³. Gene counts were calculated using featureCounts ¹⁴with parameters -s 0 -t exon -g gene_name using Gencode M21 (GRCm38) annotation downloaded from (<https://www.gencodegenes.org/mouse/>). Differentially expressed genes (DEGs) were identified using R package DESeq2 v1.20 ¹⁵. Log2FoldChanges and adjusted P-values were corrected using the apeglm

¹⁶and IHW ¹⁷ packages, respectively. Genes with a Log2 fold change ≥ 1 and an adjusted p value < 0.05 were considered as differentially expressed.

Chromatin Immunoprecipitation-Sequencing (ChIP-seq)

Organoids were fixed in disuccinimidyl glutarate (DSG) (Sigma) for 45 min and subsequently in 1% of FA for 10 min. FA was quenched using Glycine 0.125 M for 5 minutes. Fixed organoids were washed two times with PBS and lysed in SDS buffer (100mM NaCl, 50mM Tris-HCl pH 8.1, 5mM EDTA pH 8, 0.3% NaN₃, 0.5% SDS). Samples were resuspended in IP buffer (100 mM NaCl, 100 mM Tris-HCl pH8.6, 0.5 mM EDTA pH8., 0.2%, NaN₃, 0.3% SDS, 1.7% Triton X-100) and sonicated using Branson sonicator. Immunoprecipitation was performed overnight at 4°C using 5 µg of anti-CTNNB1 (Cell Signaling, D10A8 8480) and 5 µg of anti-MYC (Cell Signaling, 9402). The immunocomplexes were pulled-down using protein-A sepharose beads (Life Technologies) at 4°C for 3 hours, washed 3 times with washing buffer containing 150 mM salt, and once with 500 mM salt (150 or 500 mM NaCl, 20 mM Tris-HCl pH 8.0, 2 mM EDTA pH 8.0, 0.1% SDS, 1% Triton X-100). Samples were de-crosslinked overnight in 0.1 M NaHCO₃ and 1% SDS at 65°C. Sequencing data were aligned to mouse reference genome (mm10) using Bowtie ¹⁸ favoring only unique alignments and duplicates removed for downstream analysis. Peak calling was performed with MACS2 v2.1.1 ¹⁹. Genomic peaks annotation was performed using R package ChIPpeakAnno v3.15 ²⁰, considering the promoter region major or equal to 2.5 kb around annotated TSS (transcription start site). Motif enrichment analysis was performed using JASPAR.

Supplementary references

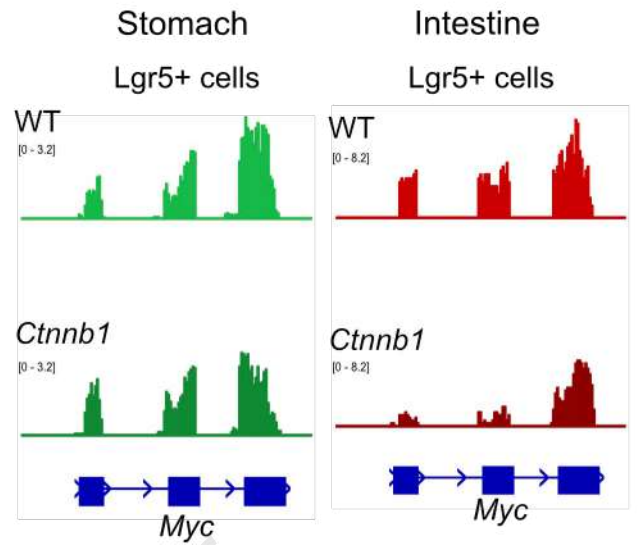
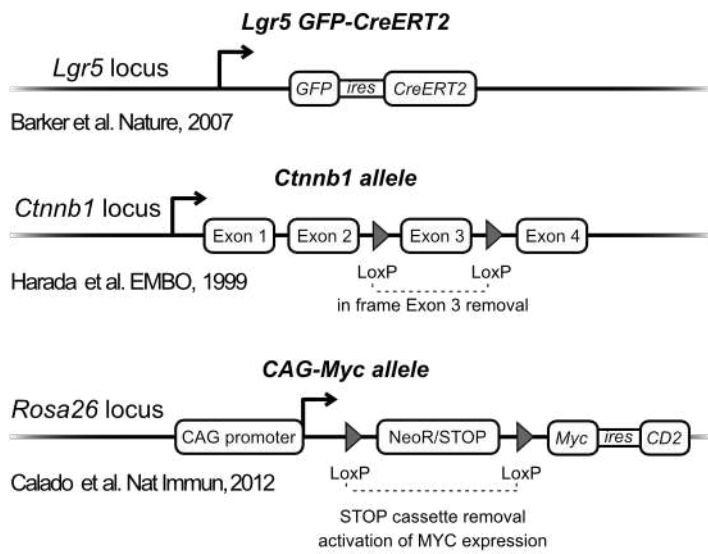
1. Harada N, Tamai Y, Ishikawa T, et al. Intestinal polyposis in mice with a dominant stable mutation of the beta-catenin gene. *EMBO J* 1999;18:5931-42.
2. Calado DP, Sasaki Y, Godinho SA, et al. The cell-cycle regulator c-Myc is essential for the formation and maintenance of germinal centers. *Nat Immunol* 2012;13:1092-100.
3. Soriano P. Generalized lacZ expression with the ROSA26 Cre reporter strain. *Nat Genet* 1999;21:70-1.
4. Barker N, van Es JH, Kuipers J, et al. Identification of stem cells in small intestine and colon by marker gene *Lgr5*. *Nature* 2007;449:1003-7.
5. Muncan V, Sansom OJ, Tertoolen L, et al. Rapid loss of intestinal crypts upon conditional deletion of the Wnt/Tcf-4 target gene c-Myc. *Mol Cell Biol* 2006;26:8418-26.
6. Meier F, Brunner AD, Koch S, et al. Online Parallel Accumulation-Serial Fragmentation (PASEF) with a Novel Trapped Ion Mobility Mass Spectrometer. *Mol Cell Proteomics* 2018;17:2534-2545.
7. Wichmann C, Meier F, Virreira Winter S, et al. MaxQuant.Live Enables Global Targeting of More Than 25,000 Peptides. *Mol Cell Proteomics* 2019;18:982-994.
8. Cox J, Hein MY, Lubner CA, et al. Accurate proteome-wide label-free quantification by delayed normalization and maximal peptide ratio extraction, termed MaxLFQ. *Mol Cell Proteomics* 2014;13:2513-26.
9. Tyanova S, Temu T, Cox J. The MaxQuant computational platform for mass spectrometry-based shotgun proteomics. *Nat Protoc* 2016;11:2301-2319.
10. Onuma K, Ochiai M, Orihashi K, et al. Genetic reconstitution of tumorigenesis in primary intestinal cells. *Proc Natl Acad Sci U S A* 2013;110:11127-32.
11. Stuart T, Butler A, Hoffman P, et al. Comprehensive Integration of Single-Cell Data. *Cell* 2019;177:1888-1902.e21.
12. Hafemeister C, Satija R. Normalization and variance stabilization of single-cell RNA-seq data using regularized negative binomial regression. *Genome Biol* 2019;20:296.
13. Faust GG, Hall IM. SAMBLASTER: fast duplicate marking and structural variant read extraction. *Bioinformatics* 2014;30:2503-5.
14. Liao Y, Smyth GK, Shi W. featureCounts: an efficient general purpose program for assigning sequence reads to genomic features. *Bioinformatics* 2014;30:923-30.
15. Love MI, Huber W, Anders S. Moderated estimation of fold change and dispersion for RNA-seq data with DESeq2. *Genome Biol* 2014;15:550.

16. Zhu A, Ibrahim JG, Love MI. Heavy-tailed prior distributions for sequence count data: removing the noise and preserving large differences. *Bioinformatics* 2019;35:2084-2092.
17. Ignatiadis N, Klaus B, Zaugg JB, et al. Data-driven hypothesis weighting increases detection power in genome-scale multiple testing. *Nat Methods* 2016;13:577-80.
18. Langmead B, Trapnell C, Pop M, et al. Ultrafast and memory-efficient alignment of short DNA sequences to the human genome. *Genome Biol* 2009;10:R25.
19. Zhang Y, Liu T, Meyer CA, et al. Model-based analysis of ChIP-Seq (MACS). *Genome Biol* 2008;9:R137.
20. Zhu LJ, Gazin C, Lawson ND, et al. ChIPpeakAnno: a Bioconductor package to annotate ChIP-seq and ChIP-chip data. *BMC Bioinformatics* 2010;11:237.
21. Van der Flier LG, Sabates-Bellver J, Oving I, et al. The Intestinal Wnt/TCF Signature. *Gastroenterology* 2007;132:628-32.

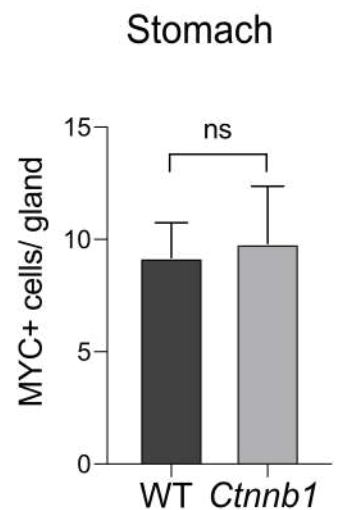
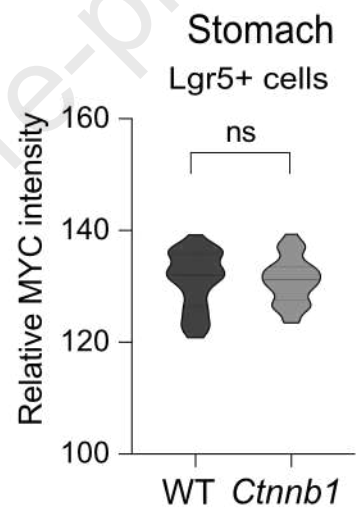
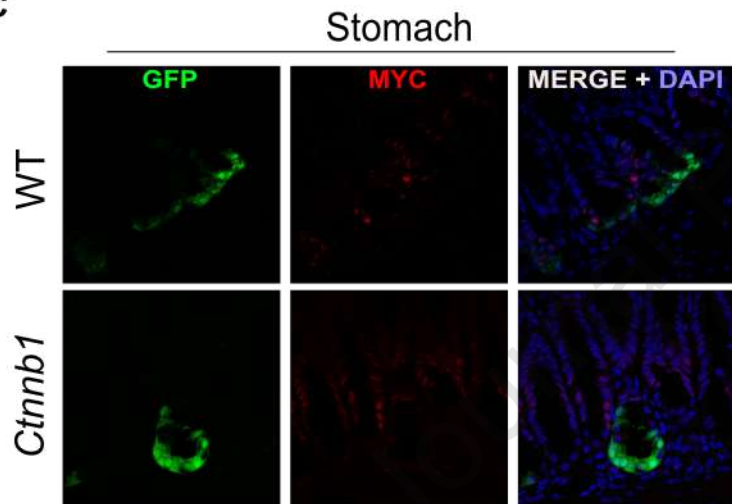
Supplementary figures and legends

Journal Pre-proof

A



C



D

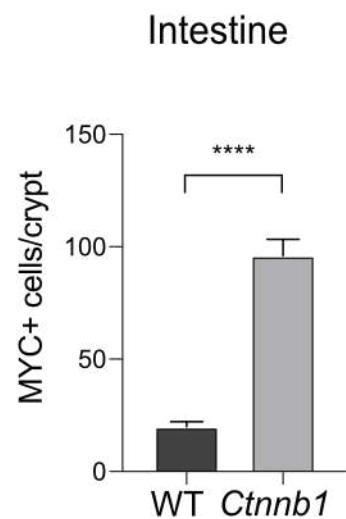
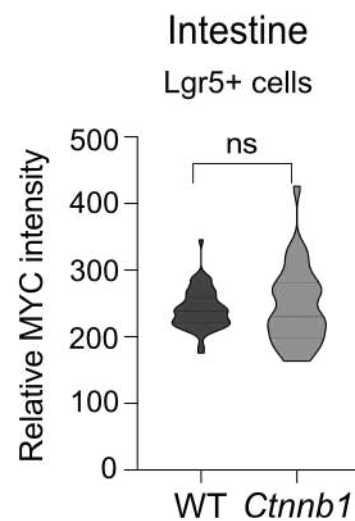
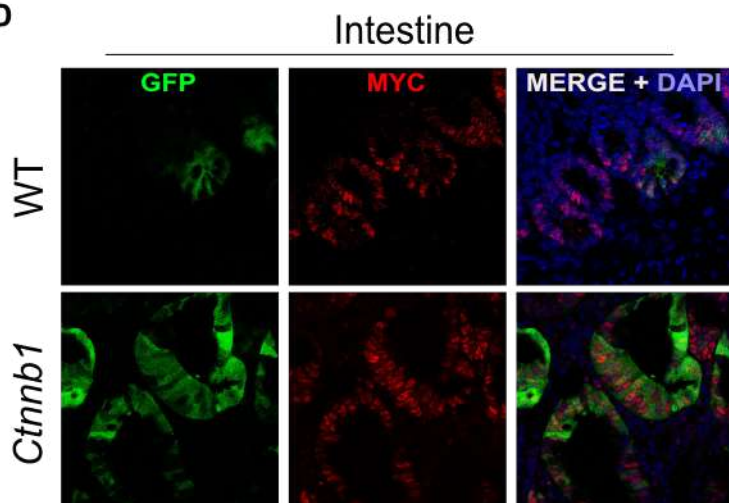


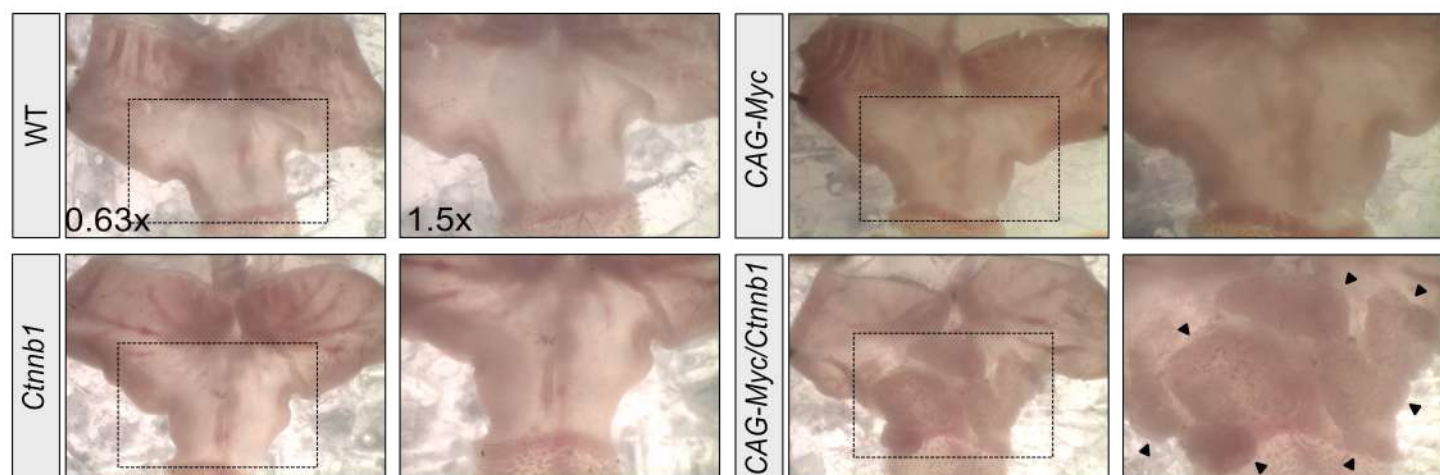
Figure S1: *Myc* expression is not induced by WNT activation in both stomach and intestinal epithelia

- A)** Schematic representation of the mouse alleles used in this study. *Lgr5 GFP-CreERT2* is a knock-in (KI) allele to express both GFP and CreERT2 by the stem cells specific *Lgr5* endogenous promoter. The *Ctnnb1* allele is a conditional allele containing two LoxP sites flanking *Ctnnb1* exon 3 that constitutively activates CTNNB1 by Cre-dependent in frame exon 3 deletion. The *Rosa26 CAG-Myc* is a KI conditional allele in which the *Rosa26* locus was engineered to conditionally express MYC and human CD2 (hCD2) under the control of a STOP cassette flanked by LoxP sites and an exogenous CAG promoter.
- B)** Genomic snapshot of RNA-seq tracks at the *Myc* locus in *Lgr5*⁺ cells derived from stomach (left) and intestine (right) of *Lgr5* GFP-CreERT2 WT and *Ctnnb1* mice 21 days PTI.
- C)** MYC staining in gastric cryosections derived from WT and *Ctnnb1* *Lgr5*-GFP-CreERT2 mice. Nuclei were counterstained with DAPI (left). Violin plots show MYC fluorescence intensity quantifications in *Lgr5*⁺ cells (middle). Quantification of the number of MYC⁺ cells per gland in the indicated mice (right). *P*-values were determined by non-parametric T-test.
- D)** As in C in small intestinal cryosections. **** indicates a *P* value < .0001.

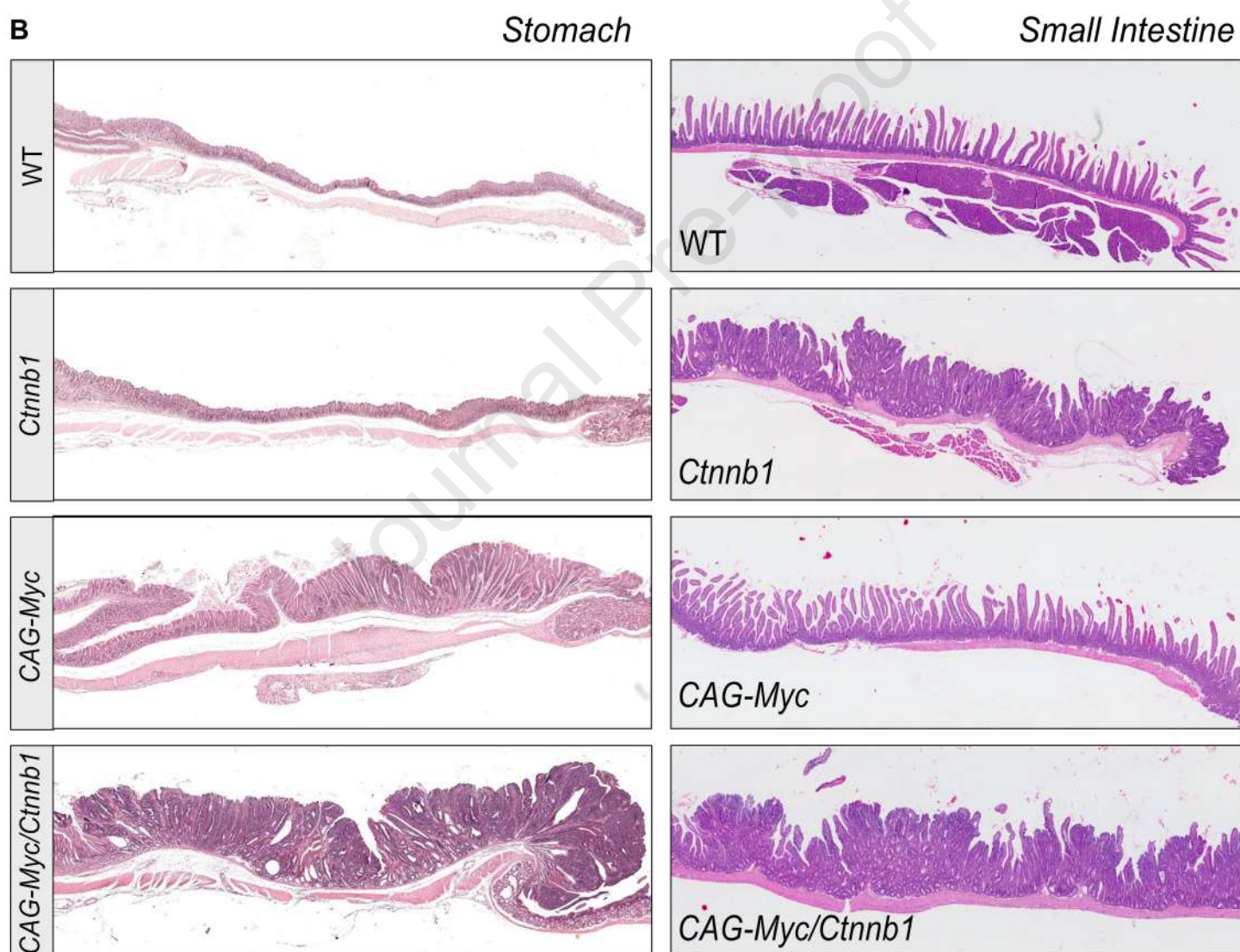
Figure S2

Journal Pre-proof
Lgr5 GFP-CreER^{1/2}

A



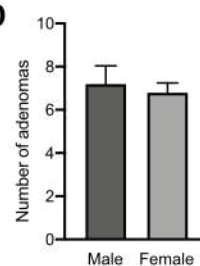
B



C

Group	n	Hyperplasia		Adenoma		Adenocarcinoma
		Simple	Atypical	Low grade	High grade	
WT	5	0	0	0	0	0
Ctnnb1	10	0	0	0	0	0
CAG-Myc	10	2	7	1	0	0
CAG-Myc/Ctnnb1	10	0	0	0	10	0

D



E

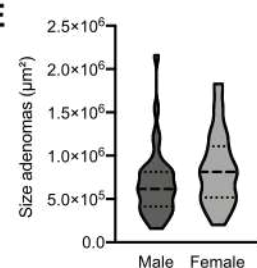


Figure S2: CTNNB1 and MYC cooperate to drive gastric tumors

- A) Stereomicroscope images of stomachs from *Lgr5 GFP-CreERT2* indicated mice at 30 days PTI. Black arrows highlight tumor formations in the gastric pyloric region of *CAG-Myc/Ctnnb1* mice.
- B) H&E staining of stomach pyloric (left) and small intestinal (right) sections from the indicated *Lgr5 GFP-CreERT2* mice at 30 days PTI.
- C) Histological evaluation of stomachs from the indicated mice and classification of gastric lesions according to Nolte et. al. 2016.
- D) Quantification of number of adenomas in the gastric pyloric region of *CAG-Myc/Ctnnb1* mice according to sex.
- E) Size of adenomas in the gastric pyloric region of *CAG-Myc/Ctnnb1* mice depending on the sex.

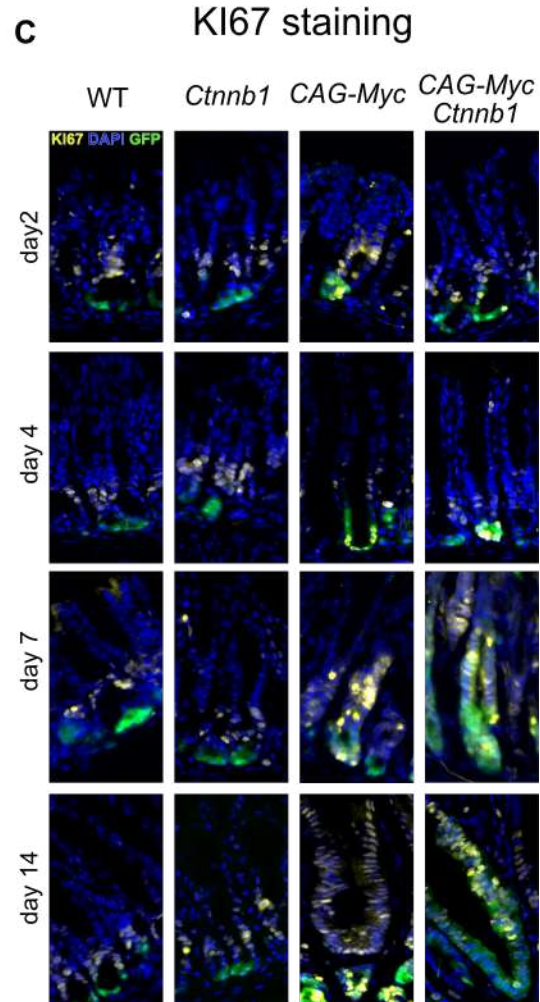
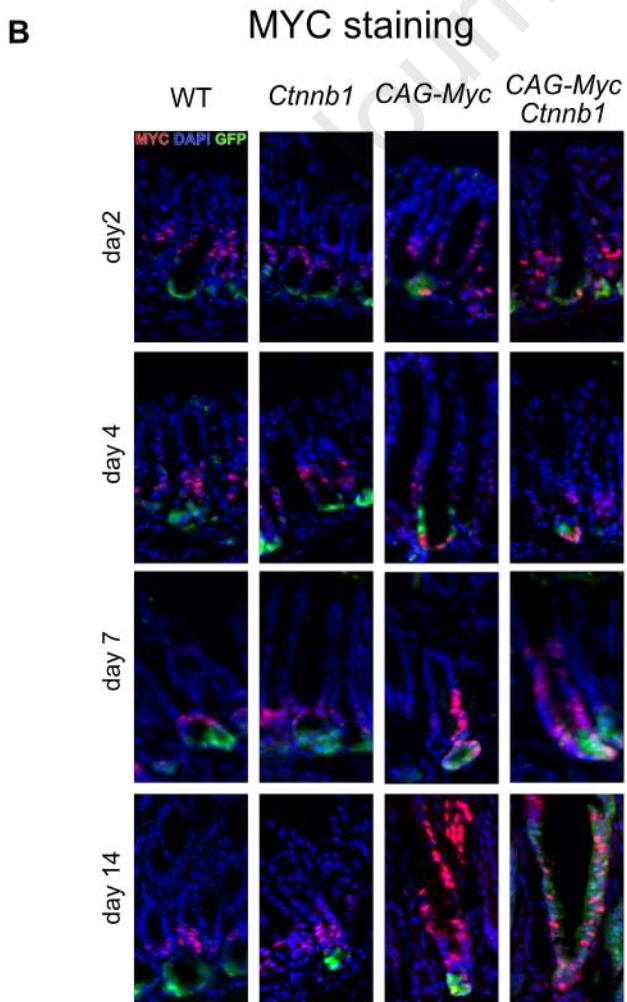
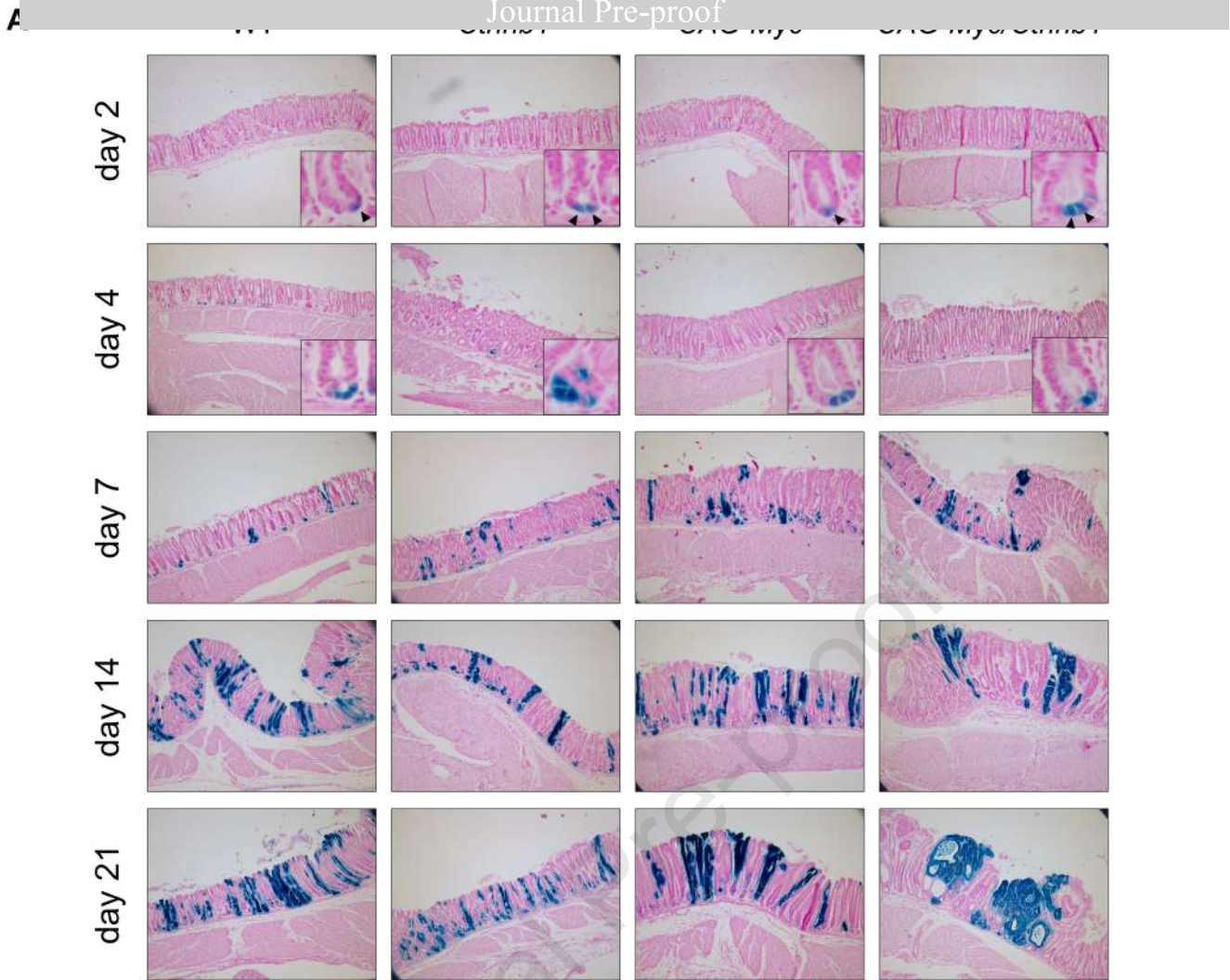


Figure S3: Transgene activation occurs in *Lgr5*+ gland base cells

- A) LacZ staining of gastric pyloric regions from the *Lgr5 GFP-CreERT2* indicated mice after 2, 4, 7, 14, 21 days PTI.
- B) MYC staining of gastric pyloric regions from the *Lgr5 GFP-CreERT2* indicated mice after 2, 4, 7, 14 days PTI.
- C) KI67 staining of gastric pyloric regions from the *Lgr5 GFP-CreERT2* indicated mice after 2, 4, 7, 14 days PTI.

Figure S4

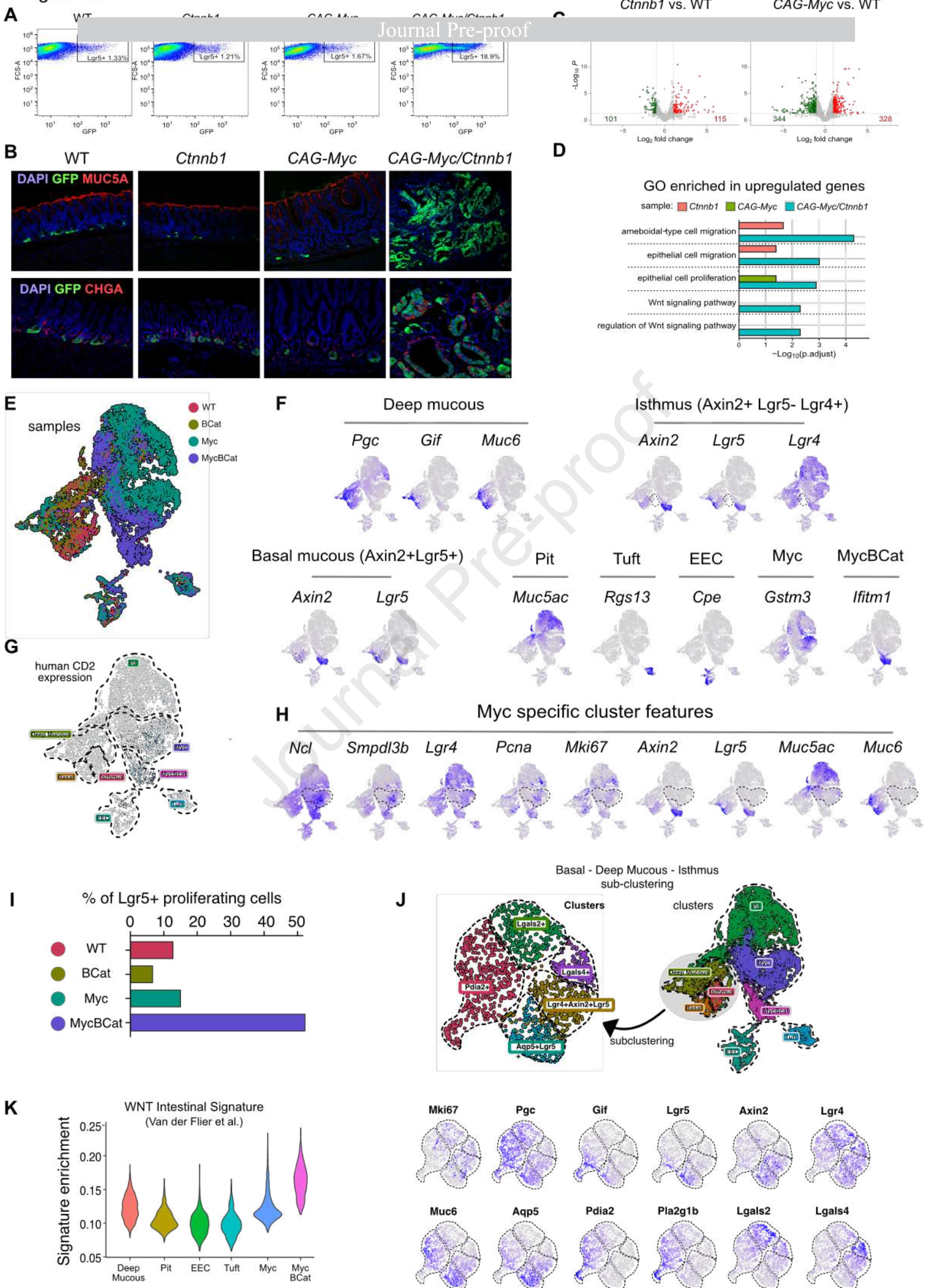
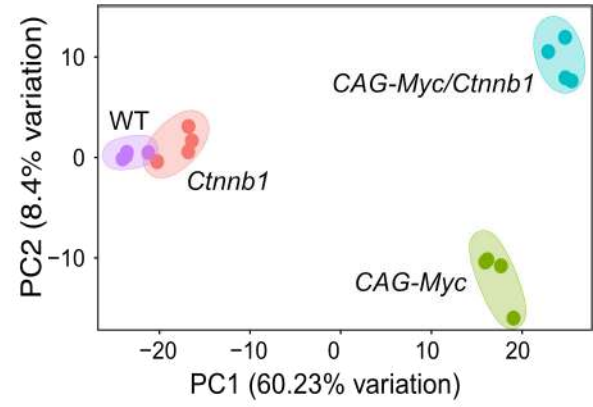
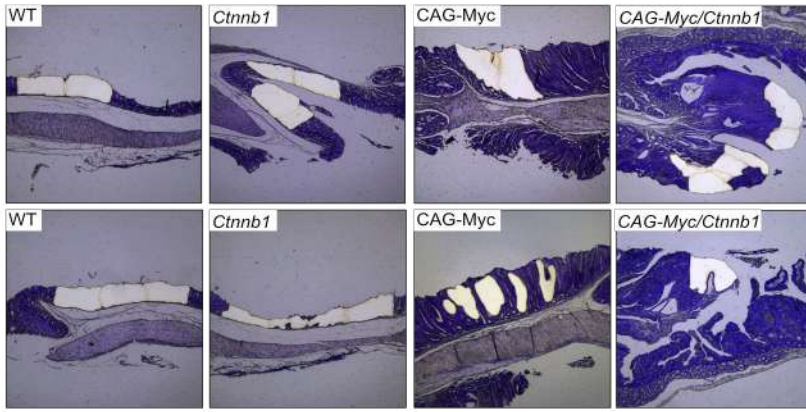


Figure S4: MYC and CTNNB1 cooperate to expand *Lgr5*+ GC suppressing the differentiation

- A)** FACS plots showing the percentage of GFP+ cells from the gastric pyloric regions of the indicated mice 21 days PTI.
- B)** IF staining for MUC5AC (marker of Pit cells) and CHGA (marker of EEC) in the gastric regions of the indicated mice. GFP shows the *Lgr5*+ GC and DAPI counterstain the nuclei.
- C)** Volcano plots showing the DEGs in the *Lgr5*+ GC RNA-seq data of the indicated confronts.
- D)** Gene Ontologies (GO) of upregulated genes in the *Lgr5*+ GC RNA-seq data of the indicated samples.
- E)** scRNA-seq UMAP plot showing the overlap between *Epcam*+ cells of the gastric pyloric regions from WT, *Ctnnb1*, *CAG-Myc* and *CAG-Myc/Ctnnb1* mice 30 days PTI.
- F)** UMAP plots showing markers of the distinct epithelial cell clusters.
- G)** UMAP showing the expression of human CD2 in the gastric cell clusters.
- H)** UMAP plots showing the expression of the indicated genes in the *Myc* specific cluster.
- I)** Barplot showing the percentage of *Lgr5* proliferating cells from scRNA-seq in the indicated samples.
- J)** Basal-Deep Mucous- Isthmus subclustering (upper) and UMAP plots showing the expression of the indicated genes (below).
- K)** Enrichment score for the expression of the WNT intestinal tumor signature from Van der Flier et al 2006²¹ across the gastric cell clusters.

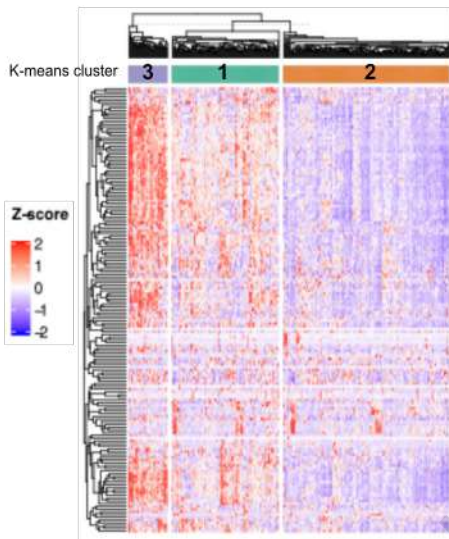
A

Laser Capture Microdissection



C

TCGA Gastric Tumors



D

MycBcat signature

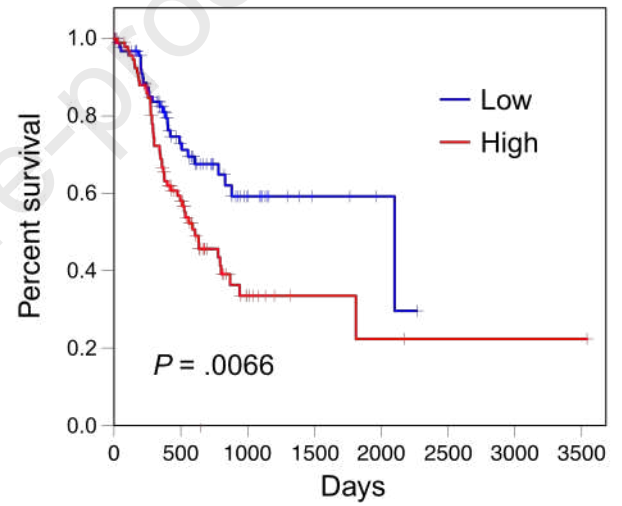


Figure S5: The MycBCat signature marks the neoplastic areas and is enriched in Gastric Human Tumors

- A) Micro-dissected areas from gastric pyloric sections stained with Cresyl-violet from the indicated *Lgr5 GFP-CreERT2* mice at 30 days PTI.
- B) Principal component analysis (PCA) of the LCM Mass Spectrometry analysis based on normalized intensity values from the micro-dissections showed in Figure A.
- C) Z-score stratification of Gastric tumors retrieved from the TCGA dataset relative to the MycBcat cluster expression signature.
- D) Kaplan-Meier plots showing the overall survival of gastric cancer patients in the TCGA cohort according to their gene expression level of the MycBcat signature. *P*-value was computed using log-rank test.

Figure S6

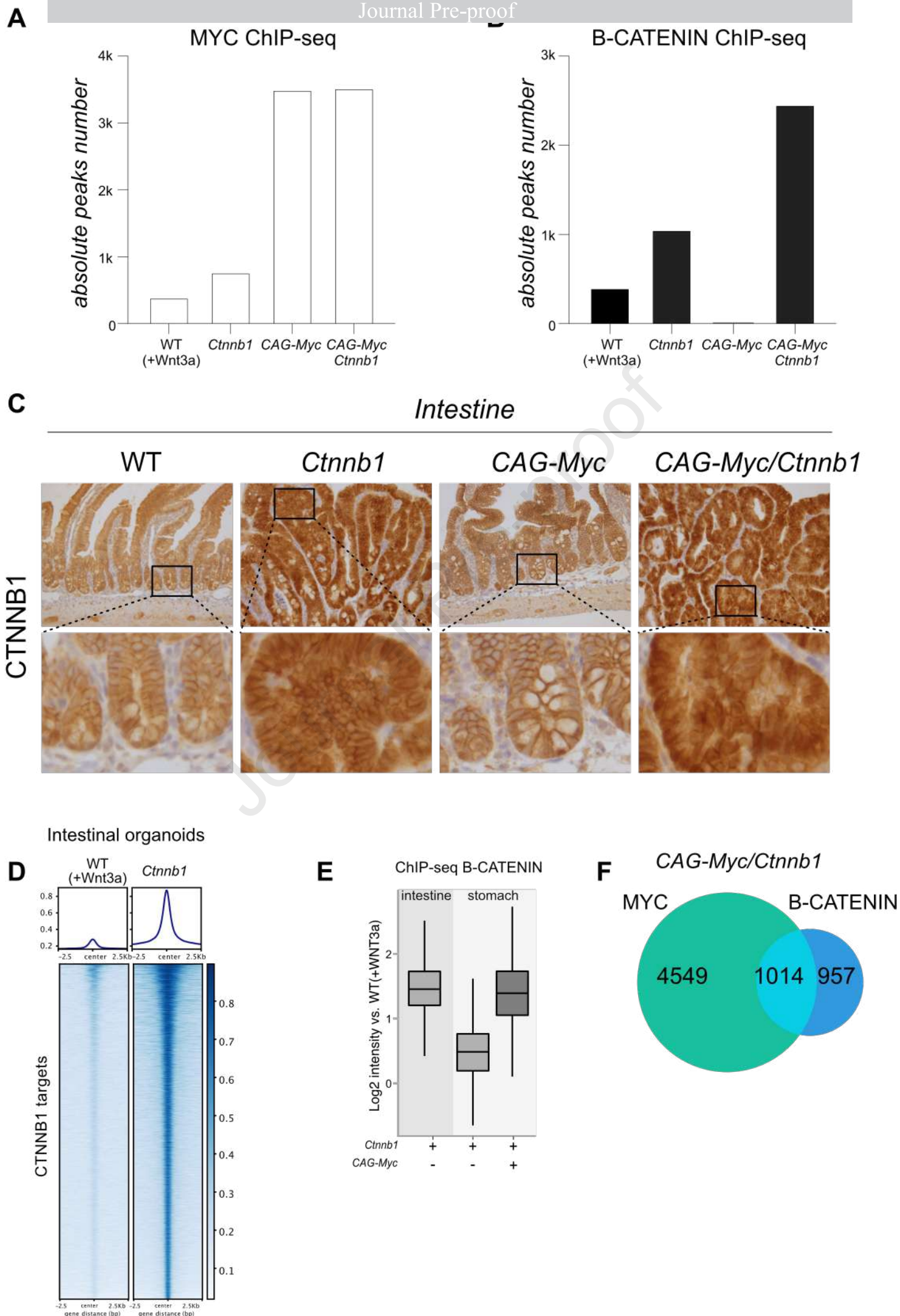


Figure S6: MYC increases the CTNNB1 chromatin accumulation

- A) Absolute number of MYC significant peaks ($-10\log_{10} p.\text{adjust} \geq 10$) identified by ChIP-seq in the indicated organoid cultures 6 days after replating.
- B) As in A for CTNNB1 ChIP-seq analyses.
- C) IHC for CTNNB1 of small intestinal sections 30 days PTI in the indicated mice.
- D) Heatmap of CTNNB1 ChIP-seq intensities over a ± 2.5 kb region from the center of CTNNB1 peaks ($-10\log_{10} p.\text{adjust} \geq 10$) in intestinal organoids.
- E) Quantification of CTNNB1 ChIP-seq intensities of *Ctnnb1* intestinal organoids and *Ctnnb1* and *CAG-Myc Ctnnb1* gastric organoids respectively vs WT (+Wnt3a).
- F) Overlap between MYC and CTNNB1 target genes classified as described in Figure 3I in *CAG-Myc Ctnnb1* gastric organoids.

Figure S7

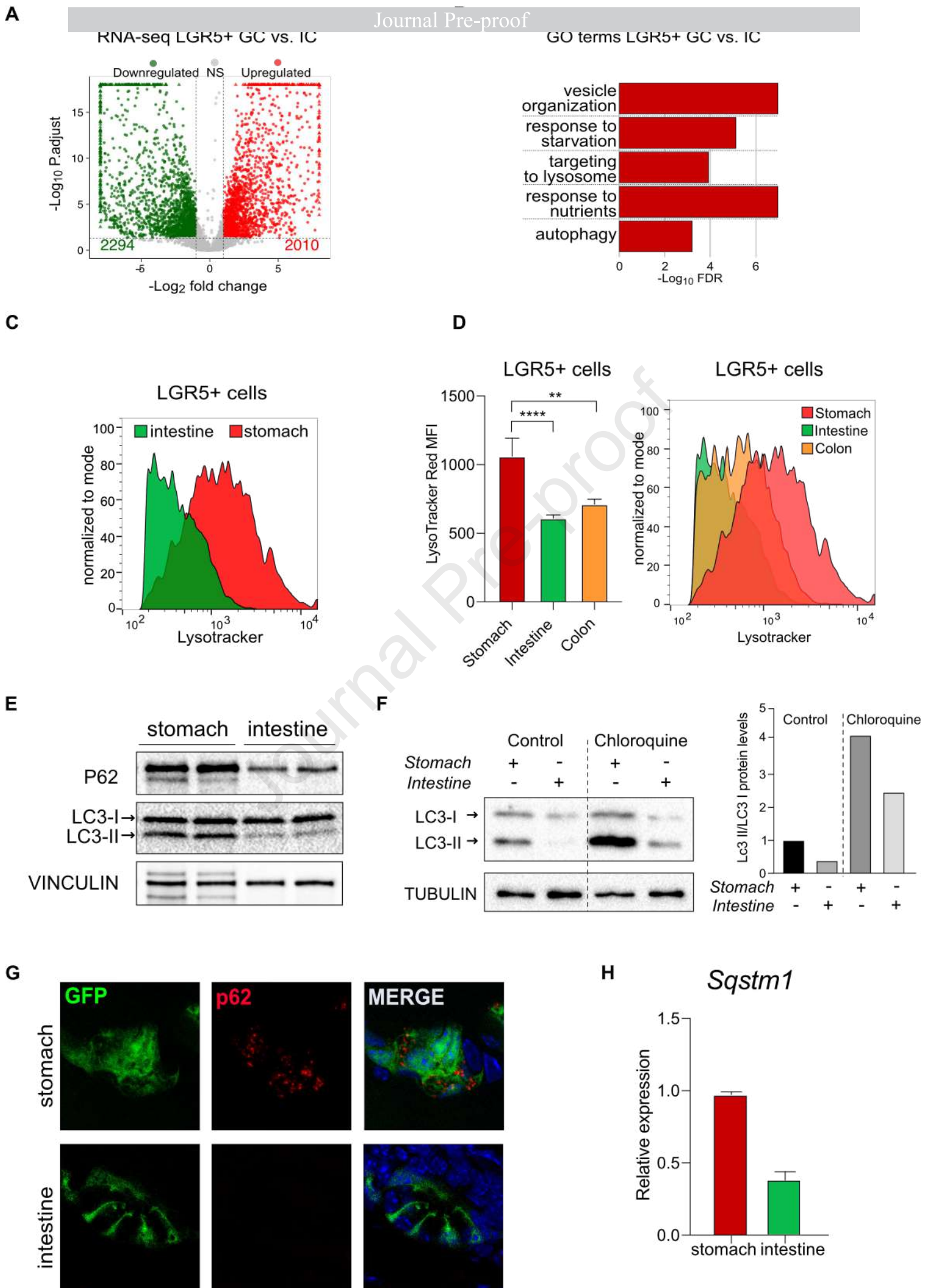


Figure S7: The stomach has high lysosomal and autophagic activity compared to the intestinal counterpart

- A)** Volcano-plots showing DEGs ($\text{Log}_2\text{FC} \geq 1$ vs. $-\text{Log}_{10} P.\text{adjust} \geq 2$) of *Lgr5+* GC vs. IC RNA-seq analysis. Upregulated DEGs are shown in red, downregulated in green and non-significant genes in gray dots.
- B)** GO analysis of upregulated genes in A highlighting the top enriched categories.
- C)** Representative plots showing the LysoTracker-Red fluorescence intensity distribution in *Lgr5+* cells from stomach and intestine.
- D)** LysoTracker Red mean fluorescence intensity (MFI) analysed by flow cytometry of *Lgr5+* cells from gastric pylorus (stomach), small intestine (intestine) and colon. *P* values: ** $P < .01$; **** $P < .0001$.
- E)** WB of gastric pyloric glands and intestinal crypts showing the P62, LC3 levels, Vinculin was used as normalisation control.
- F)** Representative LC3 immunoblot of gastric glands and intestinal crypts treated or not with 10 μM of Chloroquine for 24 hrs to assess the autophagic flux (left). Quantification of LC3II/LC3I ratio (right).
- G)** p62 staining in gastric and intestinal cryosections. GFP highlight *Lgr5+* GC and IC respectively. DAPI is used to visualize nuclei.
- H)** Relative expression of *Sqstm1* in gastric glands and intestinal WT crypts.

Figure S8

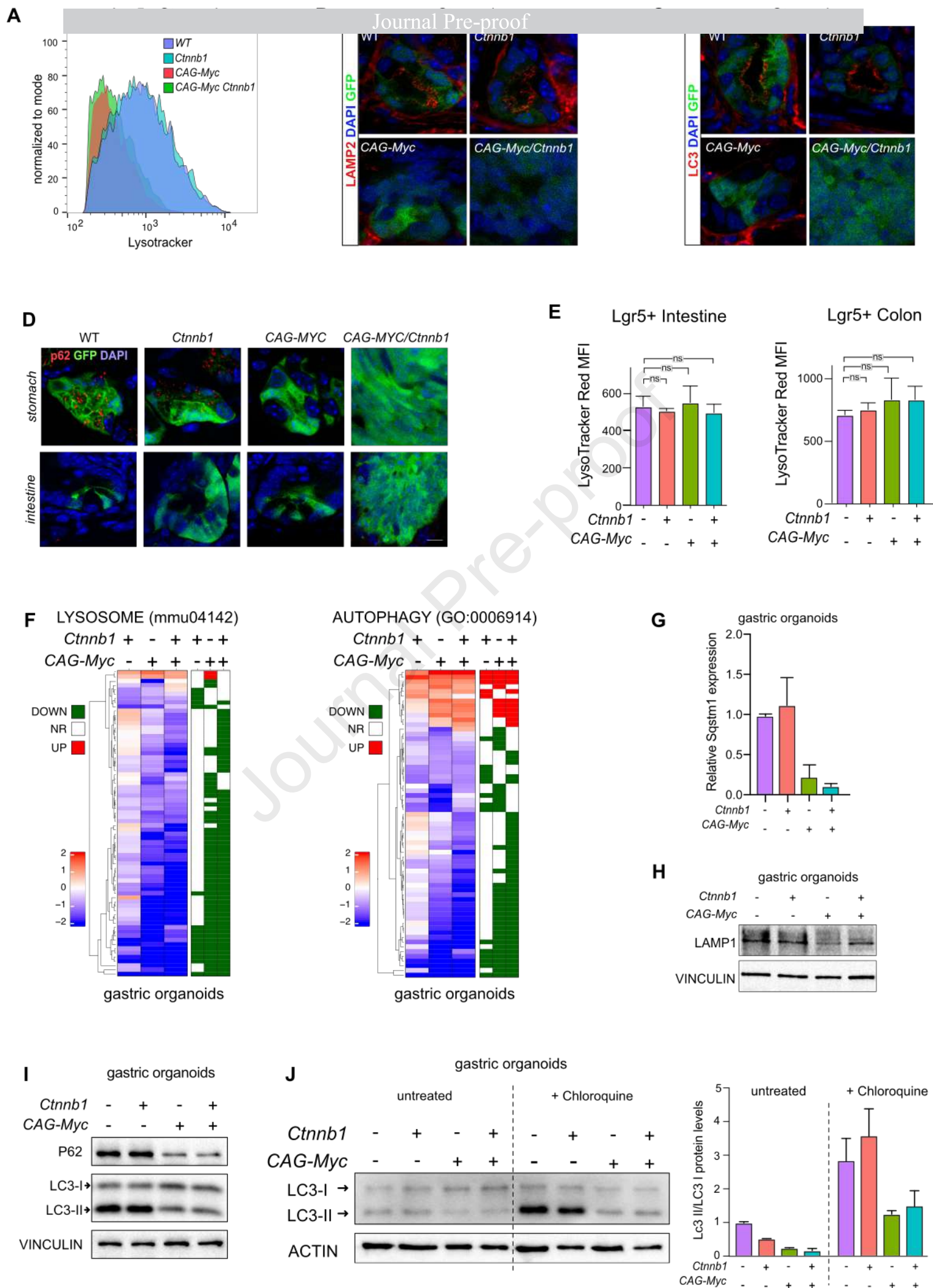
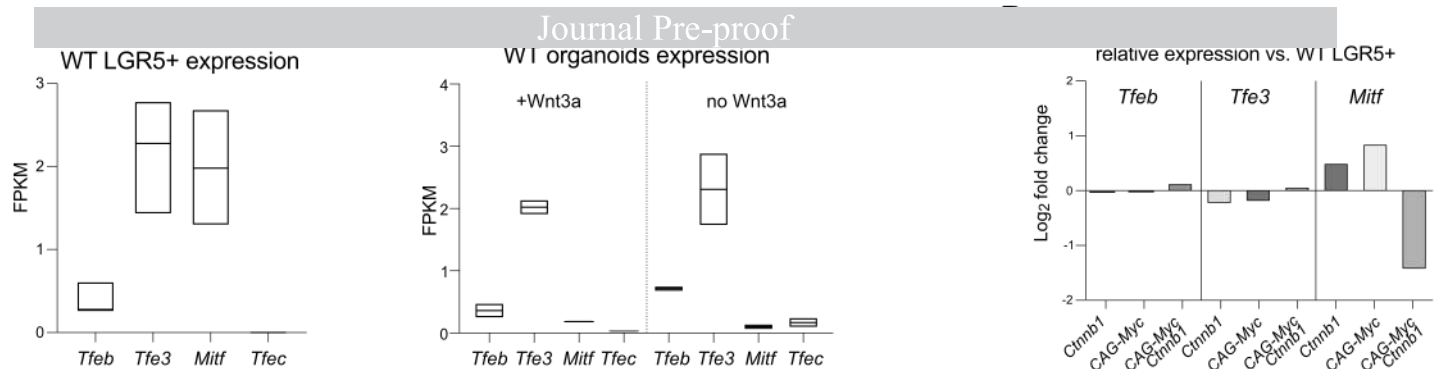


Figure S8: MYC overexpression suppresses the high lysosomal and autophagic activity of gastric tissue

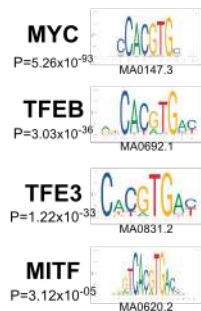
- A) Representative plots showing the LysoTracker-Red fluorescence intensity distribution in *Lgr5*⁺ GC from the indicated mice.
- B) LAMP2 staining in gastric pyloric regions from the indicated mice. GFP marks the *Lgr5*⁺ cells, DAPI counterstain the nuclei.
- C) As in B for LC3.
- D) p62 staining in gastric and intestinal cryosections. GFP highlight *Lgr5*⁺ GC and IC. DAPI is used to visualize nuclei.
- E) LysoTracker Red MFI analysed by flow cytometry of *Lgr5*⁺ cells from intestine and colon of the indicated mice.
- F) Heatmap of the Log₂ RNA-seq expression fold changes of LYSOSOME (left) and AUTOPHAGY (right) deregulated genes in *Ctnnb1*, *CAG-Myc* and *CAG-Myc/Ctnnb1* organoids relative to WT plus Wnt3a.
- G) Relative *Sqstm1* expression in gastric organoids analyzed by qPCR.
- H) WB for the lysosomal marker LAMP1 in the indicated gastric organoids.
- I) WB for P62 and LC3 in the indicated gastric organoids. VINCULIN served as loading control
- J) WB for LC3 in gastric organoids treated or not with 10 μ M of Chloroquine for 24 hrs to measure the autophagic flux (left). Boxplot showing the quantification of the LC3II/I ratio in gastric organoids (right). ACTIN served as loading control.

Figure S9

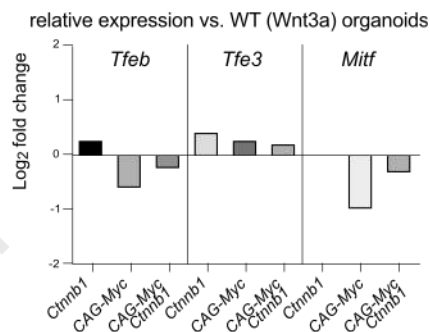
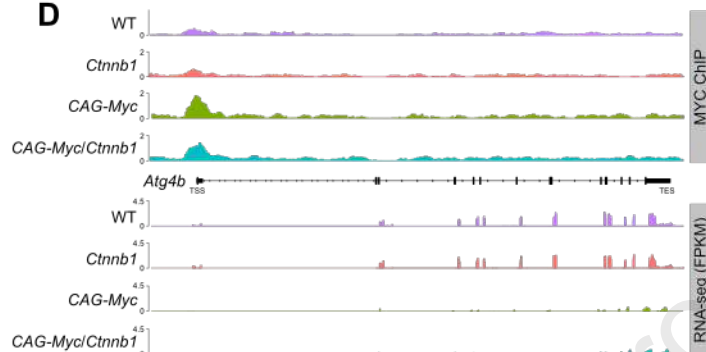
A



C

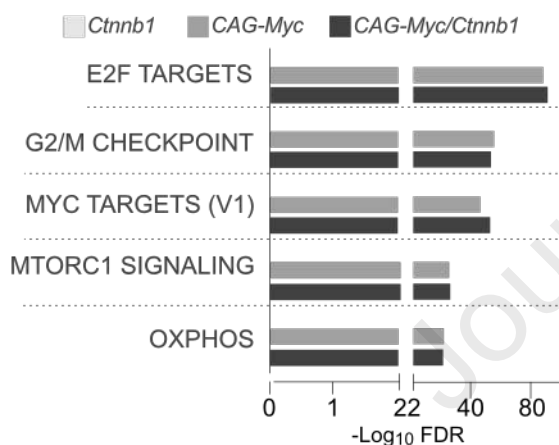


D



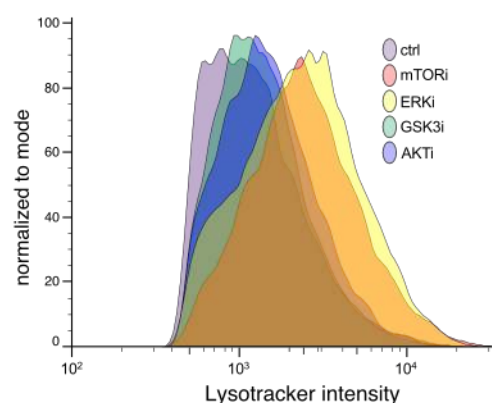
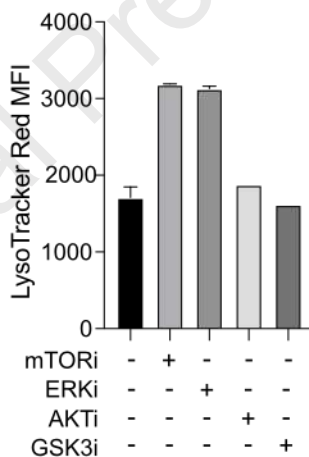
E

upregulated genes vs. WT organoids Enriched GO terms



G

CAG-Myc/Ctnnb1 gastric organoids



F

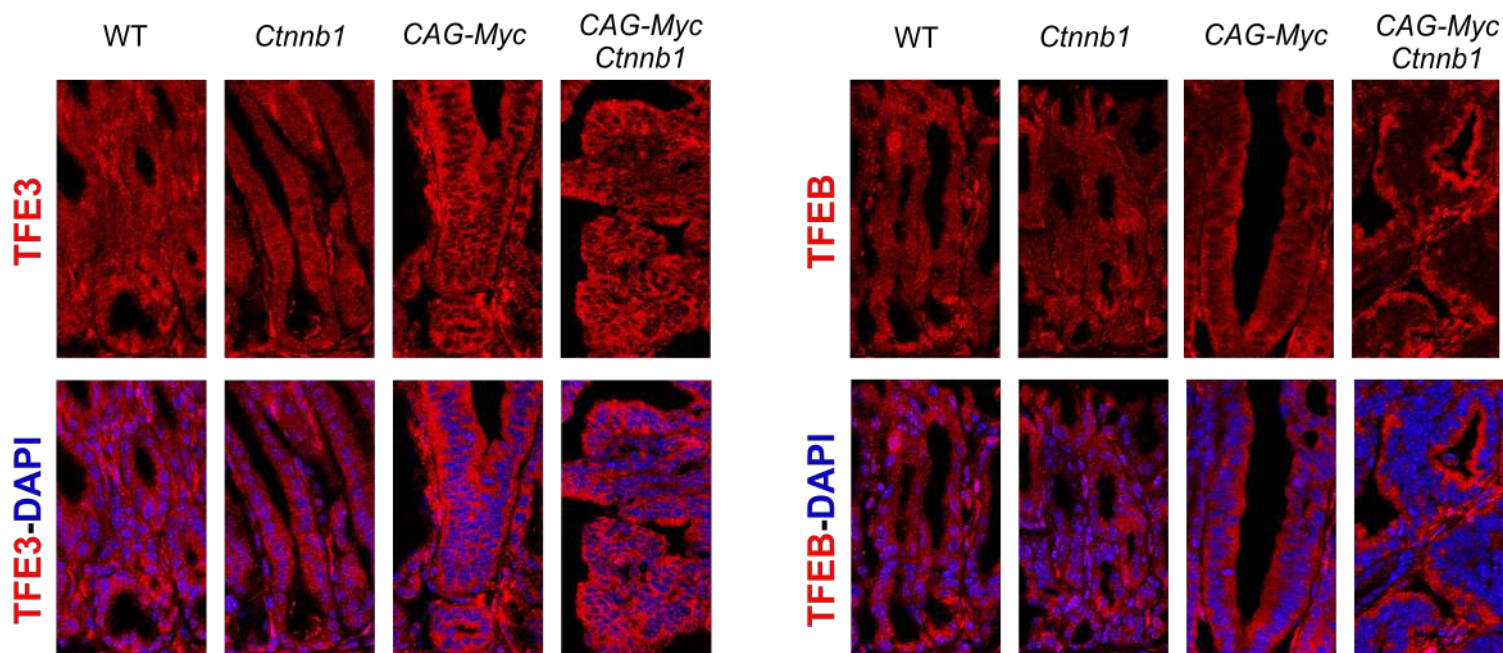


Figure S9: MYC regulates the activity of the MiT/TFE transcription factors by activating mTOR and ERK kinases

- A) Boxplot quantification of the fragments per kilobase of exon per million mapped reads (FPKM) of *Tfeb*, *Tfe3*, *Mitf*, *Tfec* RNA-seq expression in WT *Lgr5*+ GC (left) and organoids (right).
- B) Log₂ expression fold changes of *Tfeb*, *Tfe3*, *Mitf* in *Lgr5*+ GC for the indicated genotypes relative to WT (upper) and in gastric organoids (below).
- C) Motif enrichment analysis performed underneath the summit of MYC ChIP-seq *CAG-Myc/Ctnnb1* organoids peaks. Sequence weight matrices of predicted DNA binding motifs are shown together with the corresponding adjusted *P*-values.
- D) Representative ChIP-seq/RNA-seq tracks for the autophagy gene *Atg4b*.
- E) GO enrichment analysis for the RNA-seq upregulated genes from the indicated organoids relative to WT.
- F) TFE3 and TFE3 staining in gastric pyloric regions from the indicated mice 30 days PTI. Sections were counterstained with DAPI.
- G) LysoTracker Red MFI analysed by flow cytometry of *CAG-Myc/Ctnnb1* gastric organoids treated with 250 nM of Torin-1 (mTORi), 2 μM of SCH772984 (ERKi), 10 μM of LY294002 (AKTi), 5 μM of CHIR-99021 (GSK3i) for 24 hrs.

Figure S10

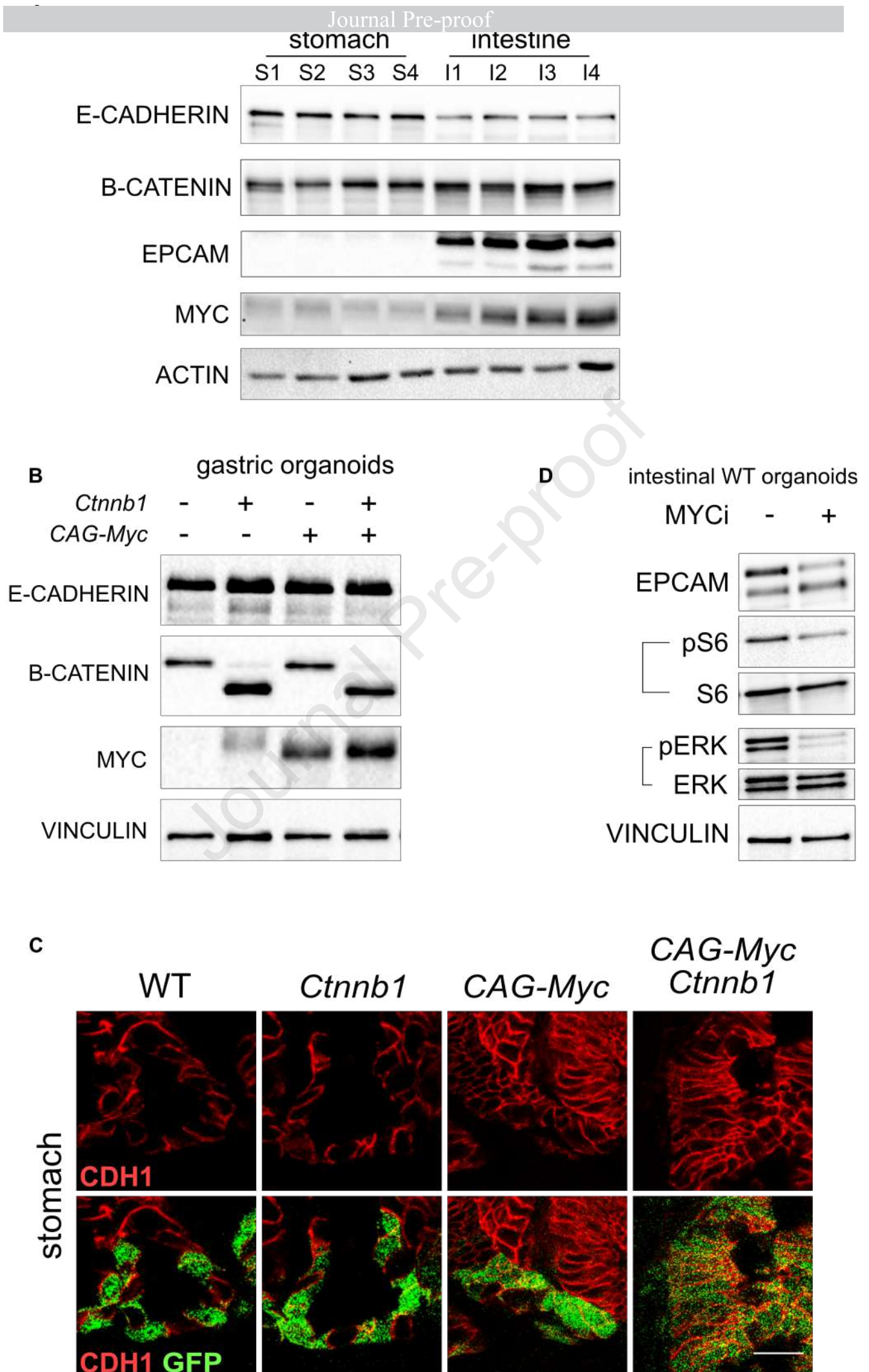


Figure S10: MYC regulates EPCAM but not CDH1 protein levels

- A)** WB analysis of WT gastric glands (stomach) and small intestinal crypts (intestine) using the indicated antibodies. S1-4 and I1-4 specify independent samples. ACTIN is presented as loading control.
- B)** Western blot analysis for the indicated proteins in gastric organoids.
- C)** CDH1 staining in gastric pyloric regions 30 days PTI.
- D)** WB for the indicated proteins in intestinal WT organoids after treatment with 50 μ M of 10058-F4 (MYCi) for 24 hrs.

Figure S11

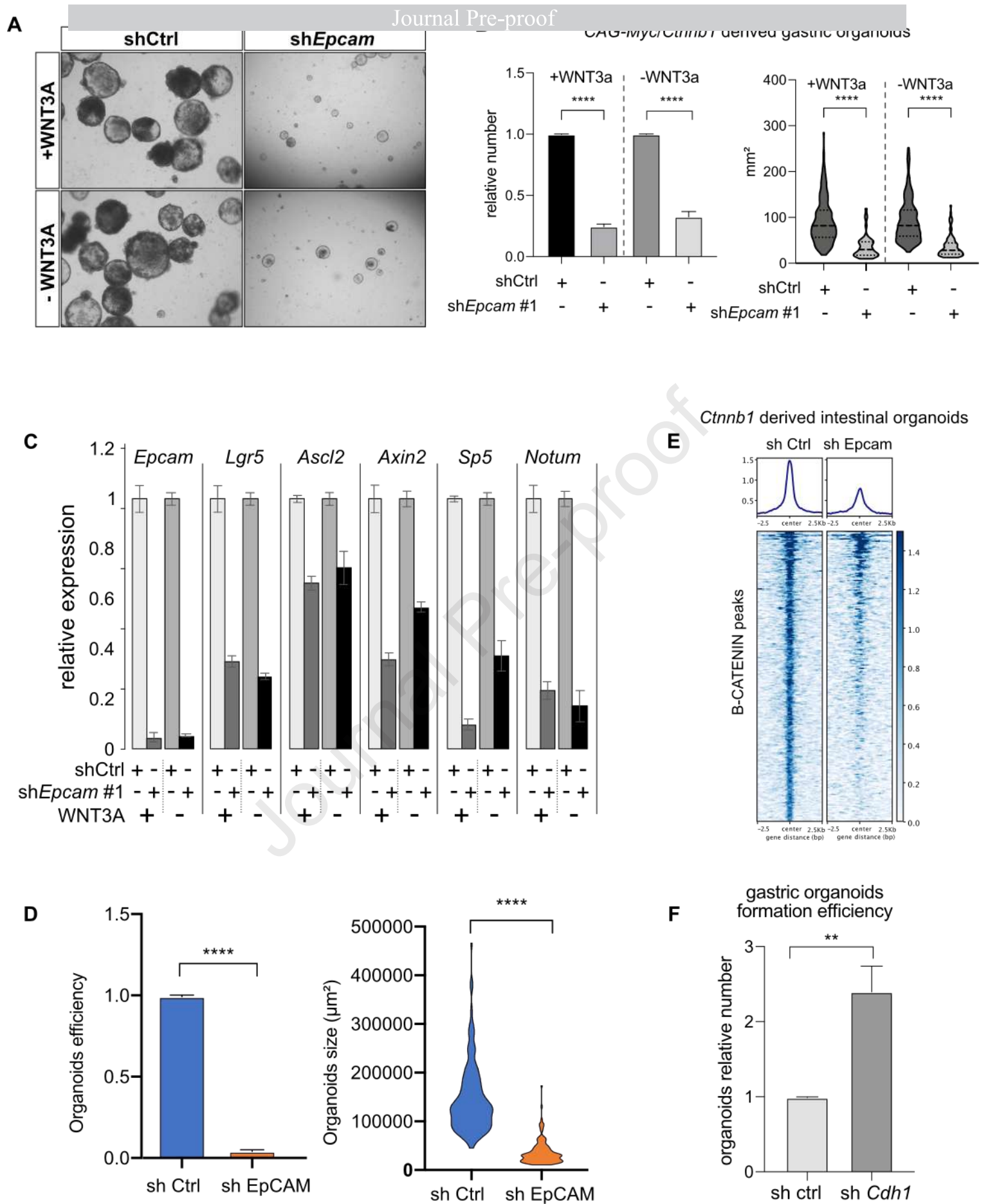


Figure S11: EpCAM regulates CTNNB1 chromatin invasion and WNT transcriptional activity

- A)** Bright field images of *CAG-Myc/Ctnnb1* gastric organoids transduced with lentiviruses expressing scramble (Ctrl) or *Epcam* shRNA in presence or absence of Wnt3a in the culture medium.
- B)** Quantification of morphology (spheroids vs budded) (left) and size (right) of organoids shown in A. **** indicates a *P* value < .0001
- C)** RT-qPCR expression analysis for the indicated genes in the organoids shown in A. *Tbp* was used as normalizing control.
- D)** Quantification of formation efficiency (left) and size (right) of intestinal *Ctnnb1* organoids shown in Figure 6F. **** indicates a *P* value < .0001
- E)** Heatmap of CTNNB1 ChIP-seq intensities over a ± 2.5 kb region across the center of CTNNB1 peaks upon *Epcam* interference in *Ctnnb1* intestinal organoids.
- F)** Quantification of formation efficiency in *Ctnnb1* gastric organoids shown in Figure 6I upon *Cdh1* interference. ** indicates a *P* value < .01

Table S1

RNA-seq data from Lgr5+ GC and IC in the indicated genotypes showing TPMs and fold-changes relative to WT control.

Table S2

List of scRNA-seq cluster gene markers classification.

Table S3

RNA-seq data from gastric organoids in the indicated genotypes showing TPMs and fold-changes relative to WT controls.

Table S4

List of identified ChIP-seq peaks for MYC and CTNNB1 in the indicated gastric organoids genotypes with related annotations.

Table S5

List of downregulated genes belonging to the Autophagy ontology (GO:0006914) and Lysosome (mmu04142) in *CAG-Myc/Ctnnb1* vs. WT gastric organoids RNA-seq analyses.

Table S6

List of primers and shRNA sequences used in this study.